Distribution Agreement

In presenting this thesis as a partial fulfillment of the requirements for a degree from Emory University, I hereby grant to Emory University and its agents the non-exclusive license to archive, make accessible, and display my thesis in whole or in part in all forms of media, now or hereafter now, including display on the World Wide Web. I understand that I may select some access restrictions as part of the online submission of this thesis. I retain all ownership rights to the copyright of the thesis. I also retain the right to use in future works (such as articles or books) all or part of this thesis.

Zijun Zhang April 13, 2021

The Investigation of the Effects of Counter-cations and Sterically Encumbered Ligands on the Structure and Catalytic Activity of Cu Complexes Supported by Bis(amidophenyl)amine Ligands

by

Zijun Zhang

Cora E. MacBeth, Ph.D.
Adviser

Chemistry

Cora E. MacBeth, Ph.D.

Adviser

Craig L. Hill, Ph.D.

Committee Member

Kurt Warncke, Ph.D.

Committee Member

2021

The Investigation of the Effects of Counter-cations and Sterically Encumbered Ligands on the Structure and Catalytic Activity of Cu Complexes Supported by Bis(amidophenyl)amine Ligands

By

Zijun Zhang

Cora E. MacBeth, Ph.D.

Adviser

An abstract of
a thesis submitted to the Faculty of Emory College of Arts and Sciences
of Emory University in partial fulfillment
of the requirements of the degree of
Bachelor of Science with Honors

Chemistry

2021

Abstract

The Investigation of the Effects of Counter-cations and Sterically Encumbered Ligands on the Structure and Catalytic Activity of Cu Complexes Supported by Bis(amidophenyl)amine Ligands
By Zijun Zhang

Bioinspired transition-metal complexes that catalyze oxidation reactions using O_2 as the terminal oxidant are heavily studied in bioinorganic chemistry. Among the metalloproteins that effectively bind and activate O_2, two kinds of type-3 copper proteins, tyrosinase and catechol oxidase, have been widely explored. In recent years, many synthetic models that both mimic the O_2 binding mode of the proteins and display tyrosinase and catecholase activities towards external substrates have been developed. Yet, more investigations can be made on the ligand steric effect and the effect of counter-ions in such bioinspired models.

In chapter 2 of this thesis, the investigation of the effect of counter-cations on the structure and catalytic activity of a copper complex supported by a bis(amidophenyl)amine ligand is reported. This bioinspired bimetallic complex displays good catalytic activity towards the aerobic oxidation of catechol. The incorporation of K^+ and $(PPh_4)^+$ as the counter-cations have been found to influence both the structure and the catalytic activity. The investigation of the difference in catalytic activity also reveals the formation of a catalytically irrelevant species in the reaction pathway.

Chapter 3 of this thesis focuses on the investigation of the ligand steric effect. Two bis(amidophenyl)amine ligands with sterically encumbered substituents are used, and two copper complexes with bridging-hydroxo ligand and one copper complex with phenolate coordination have been unexpectedly isolated. Questions about the assignment of the oxidation states of the copper centers in two of the complexes and the oxidative C-C bond cleavage of the ligand backbone in one of the complexes arise after the structural and spectroscopic characterizations. Both worth thorough investigations in future studies.

The Investigation of the Effects of Counter-cations and Sterically Encumbered Ligands on the Structure and Catalytic Activity of Cu Complexes Supported by Bis(amidophenyl)amine Ligands

By

Zijun Zhang

Cora E. MacBeth, Ph.D.

Adviser

A thesis submitted to the Faculty of Emory College of Arts and Sciences
of Emory University in partial fulfillment
of the requirements of the degree of
Bachelor of Science with Honors

Chemistry

2021

Acknowledgements

I feel extremely fortunate to have such a valuable undergraduate research experience because of all the mentorship, guidance, and support from faculty members and graduate students around me. I would like to thank Dr. Cora MacBeth for her mentorship as my advisor during my entire undergraduate research experience. Her insightful advice has made me grown so much as a researcher, and more importantly, her constant support has given me the confidence and strength to pursue a graduate study in chemistry.

The enthusiasm of both Dr. MacBeth and every member has brought a warm atmosphere to the group and made it such a great place to thrive. I would like to thank Elaine, Liu, who will soon finish her Ph.D. program, for being a great research mentor. She has guided me into research by providing careful instructions and suggestions. I cannot thank her more for taking time and effort helping me improve every one of my research talks, posters, and writings, including this thesis. I would also like to thank Dr. Dan Liu, who has recently graduated, and Ailing Yu for assisting my research, sharing valuable experience, and always being supportive.

I would also like to thank Dr. John Bacsa, our X-ray crystallographer, for his assistance with solving all the single-crystal structures for the metal complexes. His suggestions on changing methods of crystallization have made it much easier for me to obtain many of my diffraction quality crystals.

Finally, I would like to acknowledge my committee members, Dr. Craig Hill and Dr. Kurt Warncke, for providing thoughtful comments and suggestions on my thesis and thesis defense. These suggestions have given me more thoughts on my research and provided new directions for future studies.

Table of Contents

List of Figures

Chapter 1

Chapter 2

List of Tables

Chapter 2

Chapter 3

List of Schemes

Chapter 2

Chapter 3

Chapter 1. Recent Developments of Copper Complexes with Phenolase and Catecholase Activities

Introduction

Tyrosinase and catechol oxidase are both type-3 copper proteins ubiquitously found in nature, and they are responsible for various processes such as pigmentation and wound healing.[1] Tyrosinase displays phenolase activity as it catalyzes the ortho-hydroxylation of the monophenol side chain of L-tyrosine to the corresponding catechol (L-Dopa). It possesses catecholase activity as well since it can also catalyze the subsequent oxidative dehydrogenation of the catechol to quinone. On the contrary, catechol oxidase exhibits only catecholase activity.[2] Since both enzymes use naturally abundant O_2 as the oxidant, rely on an Earth-abundant metal source, and produce water as the sole byproduct, the catalytic processes are environmentally friendly and atom economic. Because of this, significant efforts in bioinorganic chemical research have been placed on the development of molecular biomimetic catalysts that perform the aerobic oxidation of phenol and catechol derivatives synthetically. This would serve as a greener alternative to traditional routes that rely on toxic oxidants and generate chemical wastes.[3, 4] Over the last few decades, a number of model complexes have been synthesized, and their reactivity towards O_2 has been tested. Direct studies of O_2 binding modes at the active site of the protein have been conducted.

Tyrosinase and catechol oxidase in nature

Both tyrosinase and catechol oxidase have a binuclear enzyme core, with each Cu center coordinated to three imidazoles of the histidine side chain. The other member of the type-3 copper protein, hemocyanin, has the same coordination mode but lacks phenolase and catecholase activities. This difference in reactivities of the three proteins in this family can be explained by

differences in the amino acid side chains in the active sites that provide different environments.[2] A study by Sugiyama and coworkers suggests that a large vacant space above the active site and the flexibility of one of the coordinating histidines that are present in tyrosinase but absent in catechol oxidase may lead to their different reactivities.[5]

All three proteins can exist in two forms: the resting form (met-form) and the oxygenated form (oxy-form). Shown below are the ligand interactions of the active site in met-tyrosinase (Figure 1-1, a) and oxy-tyrosinase (Figure 1-1, b) from *S. castaneoglobisporus*.[5] The met-form is the resting form of the enzyme, where both Cu^{II} centers are coordinated to the three histidine side chains as well as two μ-hydroxo ligands, with one hydroxo ligand stabilized by the H-bonding interaction with one nearby side chain.[6] The oxy-form is the O_2 binding form of the protein, and O_2 is bound as a peroxo ligand in the side-on $\mu\text{-}\eta^2\text{:}\,\eta^2$ binding mode.[5]

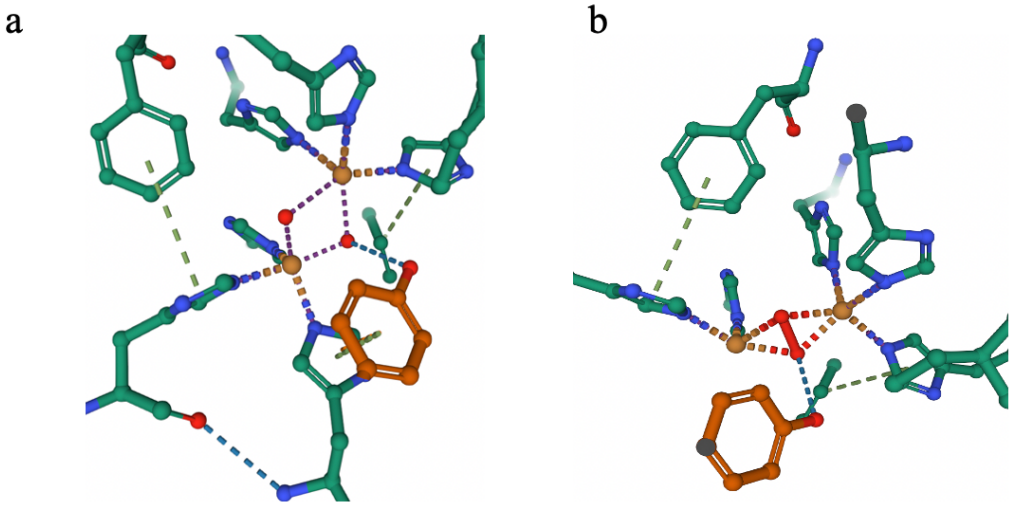

Figure 1-1. The ligand interactions at the active sites of a) met-tyrosinase and b) oxy-tyrosinase. The hydrogen atoms on the bridging hydroxide ligands in a) are omitted.

The oxy-form with the side-on bridging peroxo ligand of both the tyrosinase and the catechol oxidase is considered by many to be the active form of the protein responsible for the phenolase and catecholase activity.[2, 5] However, another form with O_2 bound as two μ-oxo ligands has also been claimed to be the active form of the protein, although no such binding mode has been isolated in crystal structures of enzymes to date. Spectroscopic characterizations of the oxy-tyrosinase has been made by Solomon, Lerch, and coworkers, indicating that the oxy-form of the tyrosinase possesses a dominant absorption feature at 345 nm and two other absorption features at 520 nm and 590 nm of lower intensity.[6] All three features are assigned as the ligand to metal charge transfer (LMCT) from the bounded oxygen to the Cu(II) center.[6] This spectroscopic characterization has been utilized in later studies of the Cu_2O_2 core in synthetic models as a standard of comparison, offering spectroscopic support that the oxy-form has the μ-η^2:η^2-peroxo binding mode (*vide infra*).

Early synthetic models of tyrosinase and catechol oxidase

The development of synthetic copper complexes that model tyrosinase and catechol oxidase began in the 1980s. The earliest reported example of a synthetic model containing a Cu_2O_2 core was developed by Karlin and coworkers (Figure 1-2).[7] This binuclear copper complex was first prepared by coordinating two Cu(I) centers to a bis(bipyridylamino)xylene ligand (m-XYLpy_2), which has two tridentate coordination sites linked by a m-xylyl linker. Upon O_2 addition, the complex performed intramolecular activation of the C(sp^2)-H bond on the arene linker, and a μ-hydroxo bridge between the two oxidized Cu(II) centers was formed, which was confirmed by X-ray crystallography.[7] The complex possessing the Cu_2O_2 core had absorption features at 340 nm, 370 nm, and 635 nm,[7] which did not match well with the absorption features of the oxy-form of

the natural enzyme. However, the first spectroscopic characterization of the enzyme has not been made at that time, and the true O_2 binding mode remained unknown. Thus, further studies were also performed, focusing on developing a variety of Cu_2O_2 core of different binding modes to be structurally and spectroscopically characterized.

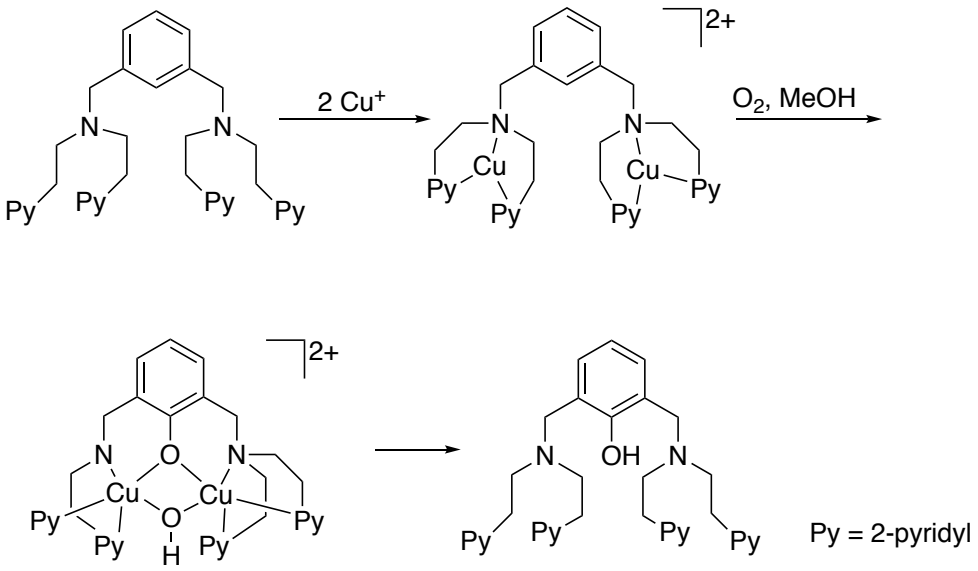

Figure 1-2. Formation of the first tyrosinase mimetic copper complex possessing a Cu_2O_2 core.[7]

The first model complex with a Cu_2O_2 core of the μ-η^2:η^2-peroxo binding mode was synthesized and structurally characterized by Kitajima and coworkers.[8] They were able to later synthesize another model complex with altered substituents on the ligand, and this complex was both structurally and spectroscopically characterized. A tridentate tris(3,5-di-isopropyl)pyrazolylborate ligand was used to coordinate to the Cu(I) center, forming a mononuclear Cu(I) complex. Upon O_2 addition, two of these complexes are linked by O_2, forming the μ-η^2:η^2-peroxo bridge (Figure 1-3), which is confirmed by X-ray crystallography.[8] The bridged complex with the Cu_2O_2 core showed absorption features at 345 nm and 530 nm,[9] consistent with the features of the natural enzyme.

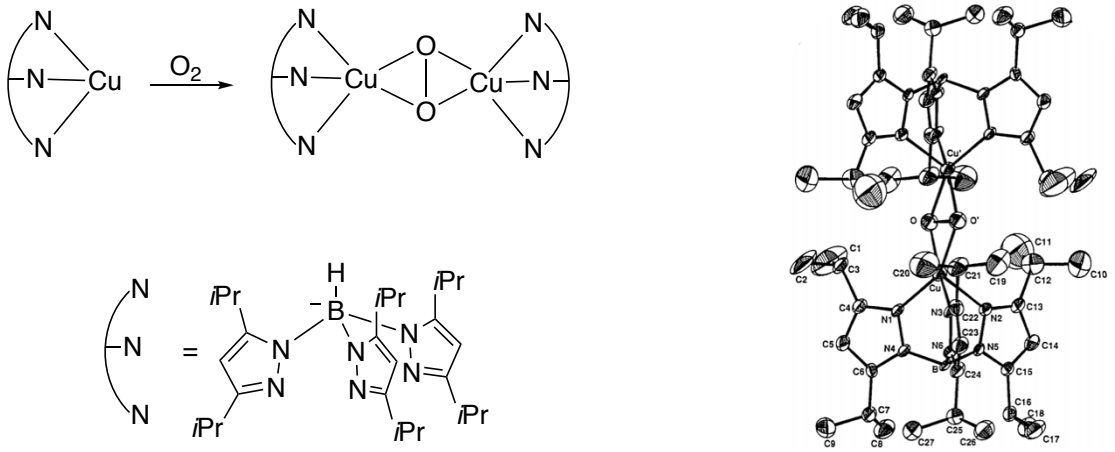

Figure 1-3. The first structurally and spectroscopically characterized Cu_2O_2 model with the μ-η^2:η^2-peroxo bridge.[9]

Around the same time, the first successful synthetic model complex capable of catalytically hydroxylating external phenol to catechol and oxidizing the catechol to quinone was developed by Réglier and coworkers. The complex is binuclear, with each Cu(I) center coordinated to two N atoms on the ligand and two MeCN solvent molecules (Figure 1-4).[10] Upon adding O_2 and Et_3N, the complex could catalyze the oxidation of 2,4-di(tert-butyl)phenol, and the formation of both the corresponding catechol and the quinone were observed, indicating that the complex possesses both phenolase and catecholase activity.[10]

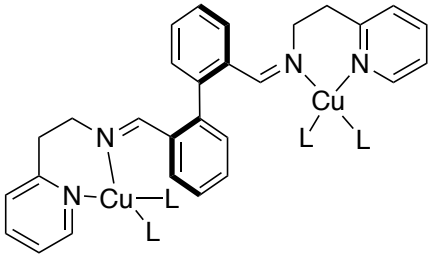

Figure 1-4. First synthetic model capable of catalyzing aerobic oxidation of external phenol and catechol.[10]

Recent developments in synthetic models

Model complexes with the μ-η²: η²-peroxo Cu_2O_2 core

More recently, the development of synthetic models has focused on forming structurally defined complexes with Cu_2O_2 cores that also display good catalytic activity. Herres-Pawlis and coworkers have developed several bis(pyrazolyl)methane-based ligands that coordinate to Cu(I) centers to form mononuclear Cu(I) precursor complexes, which, upon O_2 addition, formed the side-on μ-η²: η²-peroxo complexes (Figure 1-5).[11-13] UV-visible absorption spectra of these complexes display absorption features around 345 nm and 550 nm, with a relative intensity of 20:1. This provides spectroscopic support that the Cu_2O_2 cores have the μ-η²: η²-peroxo binding mode, and DFT calculations offer additional support of the structural assignment.[11-13] X-ray near edge absorption spectroscopy has also been used to exclude the possibility of Cu(I) or Cu(III) being the metal center, further confirming the assignment of both metal centers as Cu(II).[11] However, single-crystal structures of these complexes have not been obtained, although the reactions have been conducted at 195 K.[11-13]

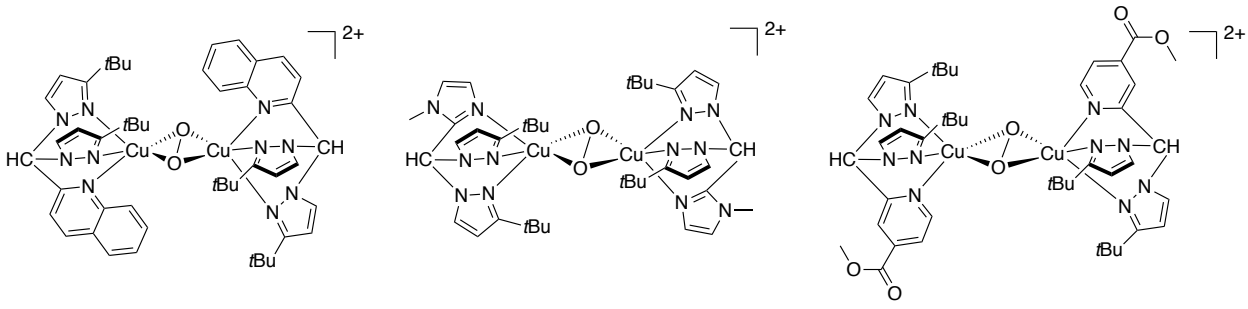

Figure 1-5. Tyrosinase model complexes with the μ-η²: η²-peroxo Cu_2O_2 cores developed by Herres-Pawlis and coworkers.[11-13]

The inability to obtain crystal structures is commonly encountered in many recent efforts to construct catalytically useful Cu_2O_2 model complexes; their high catalytic activity renders them unstable even at low temperature, making isolation of the crystalline form hard, if not impossible. The high catalytic activity of these complexes has been demonstrated by their ability to catalyze aerobic oxidations of phenol derivatives such as 8-hydroxiquinoline and para-substituted phenolates at room temperature, reaching yields up to 80%.[11, 13]

Stack and coworkers have also successfully developed model complexes with the μ-η^2: η^2-peroxo bridge. They have been able to use Cu(I) precursors coordinated to three monodentate imidazoles to form complexes with the peroxo bridged Cu_2O_2 cores (Figure 1-6).[14, 15] Again, absorption features, DFT studies, and X-ray near-edge absorption features offer support to the assignment of the peroxo binding mode, and single-crystal structure could not be obtained.[14, 15] The complex supported by 1,2-dimethylimidazole ligands (Figure 1-6, a) could catalytically oxidize several 2,4-disubstituted sodium phenolates at 148 K to the corresponding catechols with a yield up to 95%. The subsequent oxidation to quinones have also been observed at a much lower yield ($\leq$ 25%).[14]

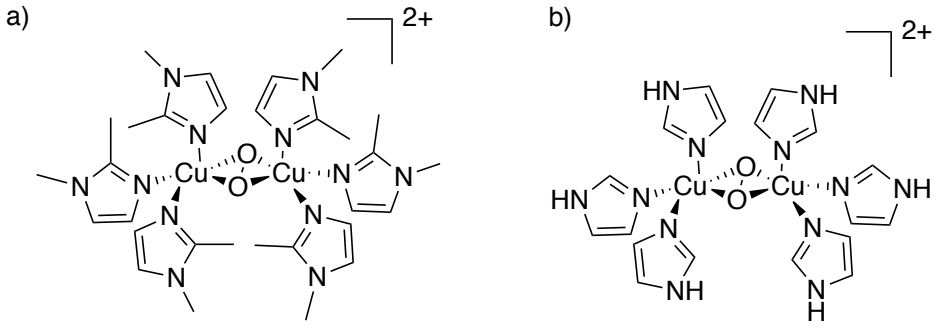

Figure 1-6. Tyrosinase model complexes with the μ-η^2: η^2-peroxo Cu_2O_2 cores developed by Stack and coworkers.[14, 15]

Model complexes with the bis(μ-oxo) Cu_2O_2 core

Although the bis(μ-oxo) coordination mode has not been observed in the oxy-form of type-3 copper proteins, studies have found that model complexes that form Cu_2O_2 cores of such coordination mode can also catalyze the aerobic oxidation of phenol derivatives successfully. It has also been suggested that the bis(μ-oxo) mode and the μ-η^2: η^2-peroxo mode of the Cu_2O_2 core are in a dynamic equilibrium in the proteins because the isomerization barrier is small,[16] and therefore, the complex with the bis(μ-oxo) could also be the active form of the catalyst.

Many complexes possessing the bis(μ-oxo) type Cu_2O_2 core have been developed, but most of them are model complexes for particulate methane monooxygenase (pMMO), another type of copper protein.[16] One complex of the bis(μ-oxo) type developed by Herres-Pawlis and coworkers has displayed tyrosinase activity, catalyzing the aerobic oxidation of several phenol and pyridinol derivatives to the corresponding quinones with very high conversion.[15] The complex has been formed by adding O_2 to a sample of mononuclear Cu(I) complex supported by a bidentate ligand (Figure 1-7).[17] The assignment of the bis(μ-oxo) binding mode is supported by DFT studies and the absorption features at 220 nm and 392 nm,[17] which are consistent with previous examples.[18] Again, the single-crystal structure of the complex could not be obtained. Although this complex shows good tyrosinase activity, the two Cu centers each coordinated to only two N atoms differs from the coordination environment in both tyrosinase and catechol oxidase. To the best of our knowledge, a model complex with the same 3N coordination mode as tyrosinase and catechol oxidase and shows good phenolase and catecholase activity has not been reported.

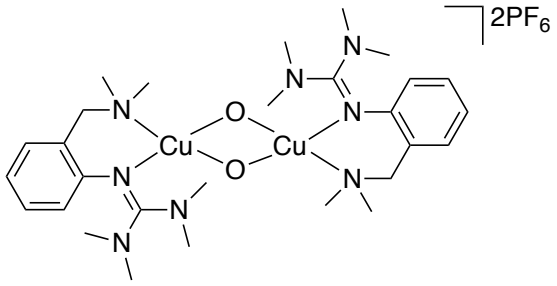

Figure 1-7. A tyrosinase model complex with the bis(μ-oxo) Cu_2O_2 cores developed by Herres-Pawlis and coworkers.[17]

Model complexes with the bis(μ-hydroxo) $Cu_2(OH)_2$ core

Although the bis(μ-hydroxido) complex is not the active oxy-form of tyrosinase and catechol oxidase, it is considered the met-form (resting form) of the protein and is related to the catalytic cycle of the enzyme. Because of this, some studies have also been done to form model complexes of the $Cu_2(OH)_2$ type. Casella and coworkers have been developing such model complexes since the 1990s and were able to obtain some early models resembling the met-form of the protein. The existence of the bridging hydroxide ligands have been confirmed by a low field peak in the ^1H NMR spectrum.[19] In a more recent example, Monzani, Casella, and coworkers have developed a catechol oxidase model $[Cu_2(mXHI)]^{4+}$ (Figure 1-8), which, upon titration with methanolic sodium hydroxide, formed the bis(μ-hydroxo) complex $[Cu^{II}_2(mXHI)(OH)_2]^{2+}$.[20] The formation of the bis(μ-hydroxo) bridge was confirmed by ^1H NMR result, which also revealed antiferromagnetic coupling of the two Cu(II) center.[20] The UV-vis spectrum of the $Cu_2(OH)_2$ complex showed absorption features at 300 nm, 350nm, and 550nm, with the former two features assigned as the hydroxide to Cu LMCT.[20] The absorption feature at 550 nm was not assigned.

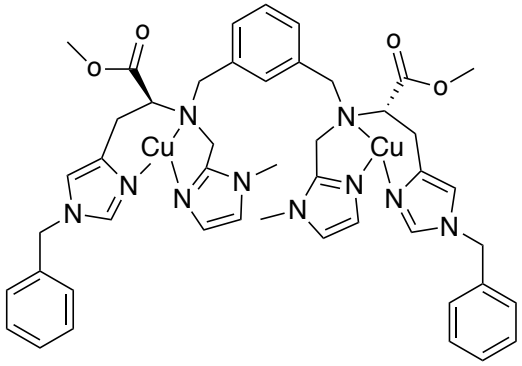

Figure 1-8. A catechol oxidase model $[Cu^{II}_2(mXHI)]^{4+}$.[20]

Reactivity and mechanistic studies

Alongside the effort of creating model complexes with well-characterized Cu_2O_2 cores, other groups have focused on trying to improve the catalytic activity of biologically-inspired complexes at room temperature. Several complexes developed by Tuczek and coworkers (Figure 1-9) were demonstrated to catalyze the aerobic oxidation of 2,4-di(tert-butyl)phenol to the corresponding quinone at room temperature when excess amount of Et_3N was added.[21, 22] However, the conversion rate of these systems is limited, with more than 50% of the starting material remaining after one hour of reaction, and the selectivity is low, as the biaryl C–C coupling product cannot be avoided.[21, 22] This formation of the coupling product suggests an off-pathway formation of the phenoxyl radical (*vide infra*), which needs to be avoided to improve the selectivity.

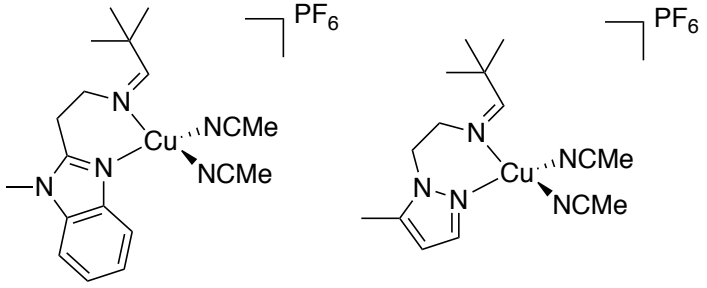

Figure 1-9. Tyrosinase model complexes developed by Tuczek and coworkers.[21, 22]

In the attempt to create copper-based complexes capable of enantioselective catalytic oxidation of catechols, Casella and coworkers have created binuclear Cu(II) complexes $[Cu_2EHI]^{4+}$ (Figure 1-10, a) and $[Cu_2L55Bu4]^{4+}$ (Figure 1-10, b).[23, 24] At room temperature, both catalysts preferably catalyze the aerobic oxidation of the L-isomer in reactions containing racemic mixtures of different catechol derivatives, and the highest enantioselectivity has been achieved when $[Cu_2L55Bu4]^{4+}$ is used to catalytically oxidize L-/D-DopaOMe (70% *ee*).[23, 24]

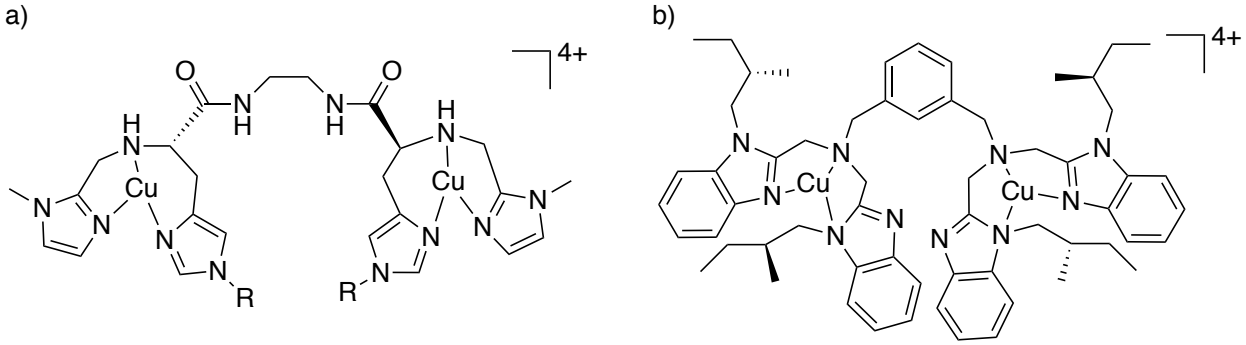

Figure 1-10. Enantioselective catechol oxidase model complexes. R = triphenylmethyl.[23, 24]

Apart from developing complexes with good catalytic activity, Itoh and coworkers have also focused on elucidating the mechanism of the conversion of phenol to catechol. In one of their studies,[25] deuterated version of the ligands L^{Py2} and L^{Py1} (Figure 1-11) originally developed by Karlin and coworkers[26] were used to construct Cu_2O_2complexes of the μ-η^2:η^2-peroxo type and the bis(μ-oxo) type respectively. Both complexes were used in catalytic aerobic oxidations of a series of lithium salts of para-substituted phenolates, which were then subjected to kinetic studies.[25] In the reaction using the μ-η^2:η^2-peroxo type complex, catechol was the sole product and no C–C coupling product was observed, and the reaction overall was pseudo-first order, dependent on the concentration of the metal complex.[25] The kinetic results together with the lack of C–C coupling product support a mechanism in which phenolate coordination to the peroxo

complex takes place prior to a electrophilic aromatic substitution step, which is considered the rate determining step (Figure 1-12, a).[25] By contrast, no reactivity was observed when the bis(μ-oxo) type complex is used.[25]

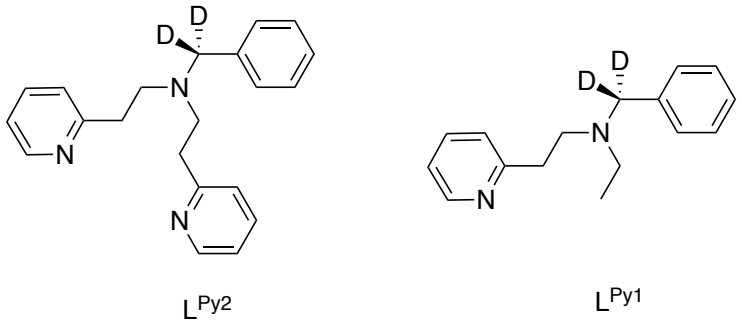

Figure 1-11. Ligands used to form Cu_2O_2 model complexes in kinetic studies by Itoh and coworkers.[25]

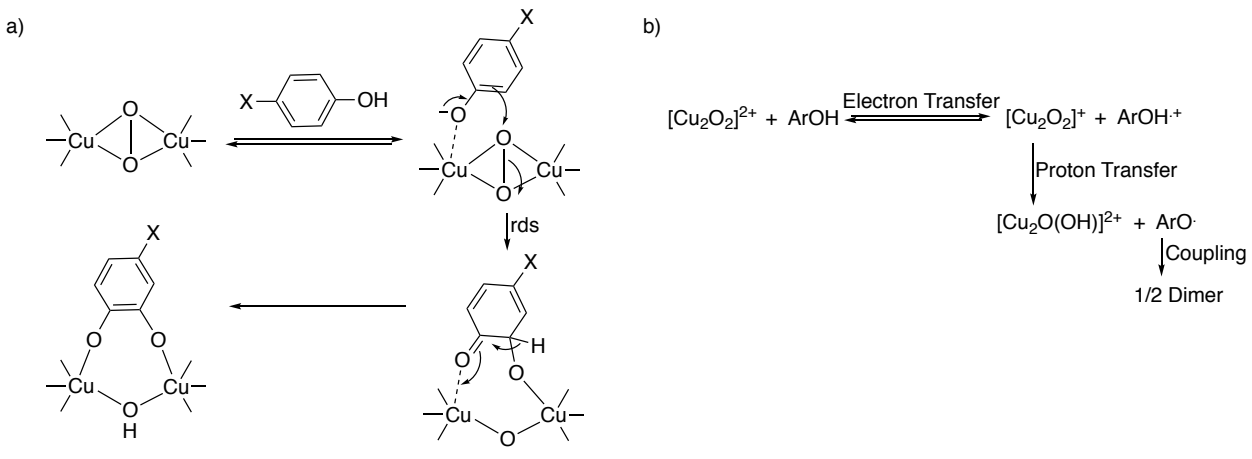

Figure 1-12. Proposed mechanisms of the catalytic aerobic oxidation of a) lithium phenolates using μ-η^2:η^2-peroxo type Cu_2O_2 complex,[25] and b) neutral phenols using μ-η^2:η^2-peroxo and bis(μ-oxo) type Cu_2O_2 complexes.[27]

In a later study by Itoh and coworkers, the same complexes were used in the catalytic aerobic oxidation of neutral para-substituted phenols.[27] This time, both complexes displayed catalytic activity, but only the biaryl, C–C coupling products were formed, and the reactions both show an overall second-order dependence on both the metal complex and the phenol substrate.[27] The results support a mechanism involving electron transfer between the Cu_2O_2 complexes and the neutral phenols to form phenoxyl radicals (Figure 1-12, b).[27] This lack of catechol formation necessitates the use of phenolate salts instead of phenol as the substrate, which is also supported by other studies, since the majority of high-yielding reactions require the use of Et_3N, which serves as the base to deprotonate the phenols. Together with the previous study on the catalytic oxidation of phenolates,[25] the reaction outcomes indicate that the coordination of the substrate to the complex is vital for catechol formation, and this coordination takes place when the phenolates are used or when bases are added.

The debate on Cu(III) species

The existence of Cu(III) species in enzymes and synthetic systems have been debated. On one hand, the Cu(III) oxidation state has been discounted because no spectroscopic evidence of its existence in biological systems has been found yet.[29] However, since the bis(μ-oxo) type Cu_2O_2 model complexes have been synthesized from the parental Cu(I) complexes, the formal oxidation state of those Cu centers in the Cu_2O_2 cores is Cu(III). In addition, in these studies that have successfully constructed the bis(μ-oxo) type core, it has been claimed that the X-ray absorption spectroscopy of the Cu K-edge displays edge positions, which are consistent with a Cu(III).[17, 29] Therefore, it is believed that in the bis(μ-oxo) type species, the Cu centers are in the Cu(III) state, and no ligand radicals exist. Apart from model complexes of tyrosinase and catechol oxidase, other biomimetic

Cu complexes have also been developed, where both hydroxo-bridged bis-Cu(III) centers and mixed-valent $Cu^{2+}Cu^{3+}$ centers have been proposed based on X-ray absorption spectroscopy, EPR spectroscopy, and DFT calculations.[30, 31]

On the other hand, in a recent study by Lancaster and coworkers, the X-ray absorption near-edge features used to prove the existence of the Cu(III) state has been disproved.[32] They propose that the edge position that was previously considered to be unambiguously assigned as the Cu 1s $\rightarrow$ 3d transition of Cu(III) could correspond to the Cu 1s $\rightarrow$ 3d of a Cu(II) center. Based on this, the X-ray absorption features used in previous studies as support of the Cu(III) state are not definitive.[32] Additionally, DFT calculations have been done in their study to show that an inverted ligand field electronic structure exists in complexes with Cu centers formally assigned as Cu(III), which means that instead of the normal ligand field, the singly occupied molecular orbital (SOMO) in such complexes have more ligand orbital characters.[31] Therefore, it is more accurate to assign the complex as a Cu(II) complex with ligand radicals. With the current debate on the existence of Cu(III) centers in both biological and synthetic systems, more investigations are still required, especially when redox non-innocent ligands are involved in the construction of such complexes.

In the following two chapters, the development of biologically-inspired Cu complexes supported by the bis(amidophenol)amine type ligands designed by the MacBeth group will be reported. Specifically, the effect of different counter-cations on the structure and catalytic activity of a bimetallic complex will be discussed, as well as the isolation and characterization of hydroxo-bridged complexes and Cu-phenolate complexes.

References

1. Kanteev, M.; Goldfeder, M.; Fishman, A. *Protein Sci.* **2015**, *24*, 1360-1369.

2. Itoh, S.; Fukuzumi, S. *Acc. Chem. Res.* **2007**, *40*, 592-600.

3. Magdziak, D.; Rodriguez, A. A.; Van De Water, R. W.; Pettus, T. R. R. *Org. Lett*. **2002**, *4*, 285-288.

4. Huang, C.; Ghavtadze, N.; Chattopadhyay, B.; Gevorgyan, V. *J. Am. Chem. Soc.* **2011**, *133*, 17630-17633.

5. Matoba, Y.; Kumagai, T.; Yamamoto, A.; Yoshitsu, H.; Sugiyama, M. *J. Biol. Chem.* **2006**, *281*, 8981-8990.

6. Himmelwright, R. S.; Eickman, N. C.; LuBien, C. D.; Lerch, K.; Solomon, E. I. *J. Am. Chem. Soc.* **1980**, *102*, 7339-7344.

7. Karlin, K. D.; Hayes, J. C.; Gultneh, Y.; Cruse, R. W.; McKown, J. W.; Hutchinson, J. P.; Zubieta, J. *J. Am. Chem. Soc.* **1984**, *106*, 2121-2128.

8. Kitajima, N.; Fujisawa, K.; Moro-oka, Y. *J. Am. Chem. Soc.* **1989**, *111*, 8975-8976.

9. Kitajima, N.; Fujisawa, K.; Fujimoto, C.; Moro-oka, Y.; Hashimoto, S.; Kitagawa, T.; Toriumi, K.; Tatsumi, K.; Nakamura, A. *J. Am. Chem. Soc.* **1992**, *114*, 1277-1291.

10. Réglier, M.; Jorand, C.; Waegell, B. *J. Chem. Soc.; Chem. Commun.* **1990**, 1752-1755.

11. Wilfer, C.; Liebhäuser, P.; Hoffmann, A.; Erdmann, H.; Grossmann, O.; Runtsch, L.; Paffenholz, E.; Schepper, R.; Dick, R.; Bauer, M. Durr, M.; Ivanovic-Burmazovic, I.; Herres-Pawlis, S. *Chem. Eur. J.* **2015**, *21*, 17639-17649.

12. Wilfer, C.; Liebhäuser, P. Erdmann, H.; Hoffmann, A.; Herres-Pawlis, S. *Eur. J. Inorg. Chem.* **2015**, 494-502.

13. Liebhäuser, P.; Kiesers, K.; Hoffmann, A.; Schnappinger, T.; Sommer, I.; Thoma, A. Wilfer, C.; Schoch, R.; Stuhrenberg, K.; Bauer, M.; Durr, M.; Ivanovic-Burmazovic, I.; Herres-Pawlis, S. *Chem. Eur. J.* **2017**, *23*, 12717-12183.

14. Citek, C.; Lyons, C. T.; Wasingerm E. C.; Stack, T. D.P. *Nat. Chem.* **2012**, *4*, 317-322.

15. Chiang, L.; Keown, W.; Citek, C.; Wasinger, E. C.; Stack, T. D. P. *Angew. Chem. Int. Ed.* **2016**, *55*, 10453-10457.

16. Elwell, C. E.; Gagnon, N. L; Neisen, B. D.; Dhar, D.; Spaeth, A. D.; Yee, G. M.; Tolman, W. B. *Chem. Rev.* **2017**, *117*, 2059-2107.

17. Paul, M.; Teubner, M.; Grimm-Lebsanft, B.; Golchert, C.; Meiners, Y.; Senft, L.; Keisers, K.; Liebhäuser, P.; Rosener, T.; Biebl, F.; Buchenau, S.; Naumova, M.; Murzin, V.; Krug, R.; Hoffmann, A.; Pietruszka, J.; Ivanovic-Burmazovis, I.; Rubhausen, M.; Herres-Pawlis, S. *Chem. Eur. J.* **2020**, *26*, 7556-7562.

18. L. M. Mirica, X. Ottenwaelder, T. D. P. Stack, Chem. Rev. 2004, 104, 1013 – 1045.

19. Casella, L.; Carugo, O. *Inorg. Chem.* **1993**, *32*, 2056-2067.

20. Lo Presti, E.; Perrone, M. L.; Santagostini, L.; Casella, L.; Monzani, E. *Inorg. Chem.* **2019**, *58*, 7335-7344.

21. Schottenheim, J.; Fateeva, N.; Thimm, W.; Krahmer, J.; Tuczek, F. *Z. Anorg. Allg. Chem.* **2013**, *639*, 1491-1497.

22. Hamann, J. N.; Tuczek, F. *Chem. Commun.* **2014**, *50*, 2298-2300.

23. Perrone, M. L.; Lo Presti, E.; Dell'Acqua, S.; Monzani, E.; Santagostini, L.; Casella, L. *Eur. J. Inorg. Chem.* **2015**, 3493-3500.

24. Perrone, M. L.; Salcadeo, E.; Lo Presti, E.; Pasotti, L.; Monzani, E.; Santagostini, L.; Casella, L. *Dalton Trans.* **2017**, *46*, 4018-4029.

25. Itoh, S.; Kumei, H.; Taki, M.; Nagatomo, S.; Kitagawa, T.; Fukuzumi, S. *J. Am. Chem. Soc.* **2001**, *123*, 6708-6709.

26. Sanyal, I.; Mahroof-Tahir, M.; Nasir, M. S.; Ghosh, P.; Cohen, B. I. Gultneh, I.; Cruse, R. W.; Farooq, A.; Karlin, K. D.; Liu, S.; Zubieta, J. *Inorg. Chem.* **1992**, *31*, 4322-4332.

27. Osako, T.; Ohkubo, K.; Taki, M.; Tachi, Y.; Fukuzumi, S.; Itoh, S. *J. Am. Chem. Soc.* **2003**, *125*, 11027-11033.

28. Gary, J. B.; Citek, C.; Brown, T. A.; Zare, R. N.; Wasinger, E. C.; Stack, T. D. P. *J. Am. Chem. Soc.* **2016**, *138*, 9986-9995.

29. Herres-Pawlis, S.; Verma, P.; Haase, R.; Kang, P.; Lyons, C. T.; Wasinger, E. C.; Flörke, U.; Henkel, G.; Stack, t. d. p. *J. Am. Chem. Soc.* **2009**, *131*, 1154-1169.

30. Halvagar, M. R.; Solntsev, P.; Lim, H.; Hedman, B.; Hodgson, K.; Solomon, E. I.; Cramer, C. J.; Tolman, W. B. *J. Am. Chem. Soc.* **2014**, *136*, 7269-7272.

31. Isaac, J. A.; Gennarini, F.; López, I.; Thibon-Pourret, A.; David, R.; Gellon, G.; Gennaro, B.; Philouze, C.; Meyer, F.; Demeshko, S.; Le Mest Y.; Réglier, M.; Jamet, H.; Le Poul, N.; Belle, C. *Inorg. Chem.* **2016**, *55*, 8263-8266.

32. DiMucci, I. M.; Lukens, J. T.; Chatterjee, S.; Carsch, K. M.; Titus, C. J.; Lee, S. J.; Nordlund, D.; Betley, T. A.; MacMillan, S. N.; Lancaster, K. M. *J. Am. Chem. Soc.* **2019,** *141*, 18506-18520.

Chapter 2. The Effect of Counter-cations on the Reactivity of a Binuclear Cu Catalyst and the Characterization of an Off-pathway Species in Aerobic Catechol oxidation

Introduction

Redox-active ligands with *N*-amidate donor moieties are widely used in coordination chemistry in part because they are strong σ-donors that can stabilize metal centers of high oxidation states.[1] Because of this, metal complexes bearing such ligands have been widely explored in oxidation catalysis.[2] In the MacBeth group, a series of bis(amidophenyl)amine type ligands that incorporate the *N*-amidate moieties have been developed (Figure 2-1). The aromatic rings of the ligand backbone allow them to act as an electron reservoir, and all three nitrogen atoms, the two amide N atoms and the amine N atom, can be deprotonated and act as σ-donors to the metal center. Additionally, the substituents of the two amides can be easily altered to offer the ligands different electronic and steric environments. The first of this type of ligand, bis(2-isobutyrylamidophenyl)amine (H_3L^{iPr}), was reported in 2011 (Figure 2-1).[2] This ligand has been used to form a binuclear Co(II) complex capable of catalyzing C-H amination and aerobic deformylation,[3,4] and it also binds and stabilizes superoxide.[4]

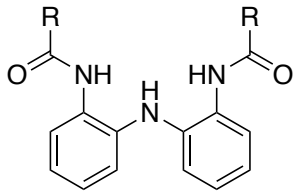

Figure 2-1. The bis(amidophenyl)amine type ligand developed by the MacBeth group. R = *i*Pr for H_3L^{iPr}.

Because this ligand has the tridentate 3N binding mode that is similar to that of tyrosinase and catechol oxidase, its coordination to Cu(II) centers has also been explored in the MacBeth group. A binuclear Cu(II) complex $[Cu_2(L^{iPr})_2]^{2-}$ was synthesized with both K^+ and $(PPh_4)^+$ as the counter-cation, and preliminary studies showed different catalytic activity towards aerobic catechol oxidation when these different counter-cations were used.[5] In order to explain the different catalytic activity, we report here the structural and spectroscopic characterization of $K_2[Cu_2(L^{iPr})_2]$ and $(PPh_4)_2[Cu_2(L^{iPr})_2]$, their catalytic activity towards the oxidation of 3,5-di(tert-butyl)catechol at different catalyst loadings, and the isolation of an off-pathway species.

Results and discussion

Ligand and complex syntheses

The ligand H_3L^{iPr} was synthesized according to the reported literature procedure.[2] The bis(nitrophenyl)amine precursor was obtained through a nucleophilic aromatic substitution between 1-fluoro-2-nitrobenzene and 2-nitroaniline, and this precursor was hydrogenated using Pd/C to form the bis(aminophenyl)amine precursor. After the acyl substitution using isobutylryl chloride, the final product H_3L^{iPr} was obtained (Scheme 2-1). A detailed procedure is provided in the experimental section.

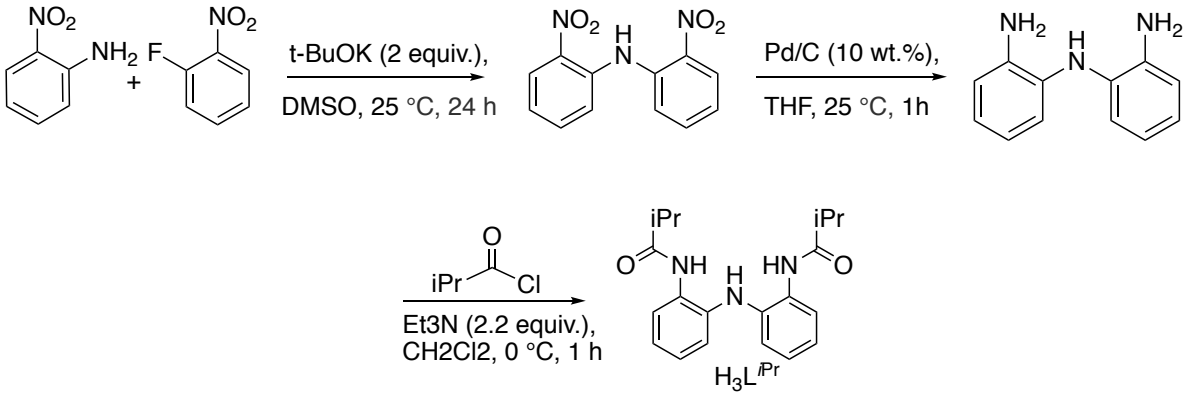

Scheme 2-1. The synthesis of ligand H_3L^{iPr}.

The ligand H_3L^{iPr} was then used in metalation reactions to form the binuclear Cu(II) complexes $(PPh_4)_2[Cu_2(L^{iPr})_2]$ (**1**) and $K_2[Cu_2(L^{iPr})_2]$ (**2**) (Scheme 2-2). The ligand was deprotonated by three equivalents of KH, and one equivalent of Cu_2Br_2 was then added to form the complex. In the formation of complex **1**, PPh_4Br was added to the reaction mixture at the same time as the addition of Cu_2Br_2. Both complexes were isolated as dark purple powder. A detailed procedure is provided in the experimental section.

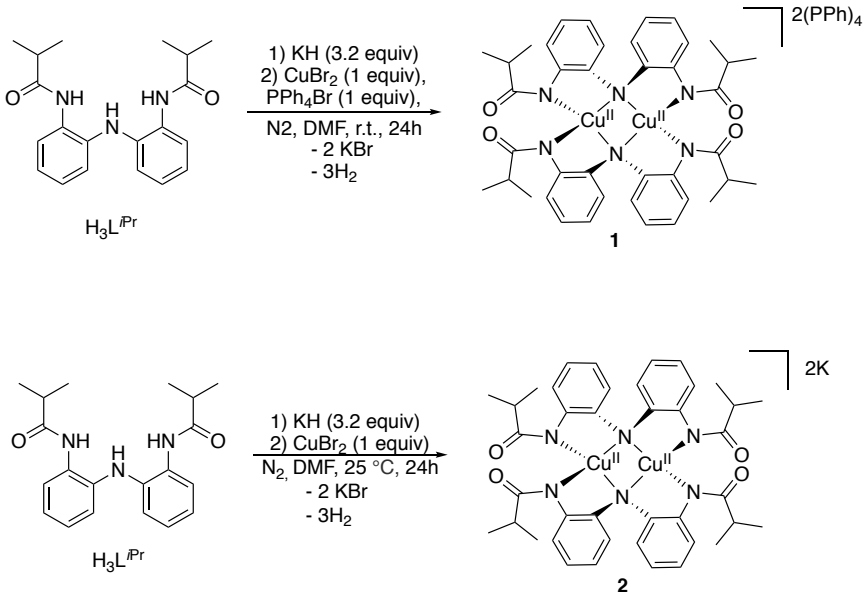

Scheme 2-2. The syntheses of complexes **1** and **2**.

Complex characterization

Single crystals of **2** suitable for X-ray diffraction were obtained by diffusing diethyl ether into a concentrated solution of the complex in tetrahydrofuran (THF). Single crystals of **1** suitable for X-ray diffraction were obtained in previous studies by diffusing diethyl ether into a concentrated solution of acetonitrile.[5] Shown below in Figure 2-2 are the single-crystal structures of complexes **1** and **2** obtained from X-ray diffraction, and the selected bond angles and bond lengths in the

single-crystal structures are displayed in Table 2-1 and Table 2-2. Both complexes have a Cu_2N_2 core, but because the K^+ counter-cations of **2** are coordinated to the ligand backbone forming a second coordination sphere, the geometry and symmetry of **2** are distorted. In **1**, the structure possesses a vertical C_2 rotation axis, and the corresponding bond lengths and bond angles for both Cu centers are the same. Each Cu center has a distorted seesaw geometry, with a τ_4 value of 0.62. The τ_4 value is a geometry index used to evaluate the geometry of four-coordinated metal centers; a perfect square plane geometry has a τ_4 of 0, a perfect tetrahedron has a τ_4 of 1, and a perfect seesaw has a τ_4 of 0.5.[6] In contrast, **2**·THF does not have the C_2 axis and is of much lower symmetry because the corresponding bond lengths and angles of the two Cu centers are different. Because of the coordinated K^+ counter-cations, significant changes in bond angles such as the N_1-Cu_1-N_4 and the N_3-Cu_2-N_6 angles are observed. Both Cu centers in **2**·THF are still of the distorted seesaw geometry, with τ_4 values of 0.64.

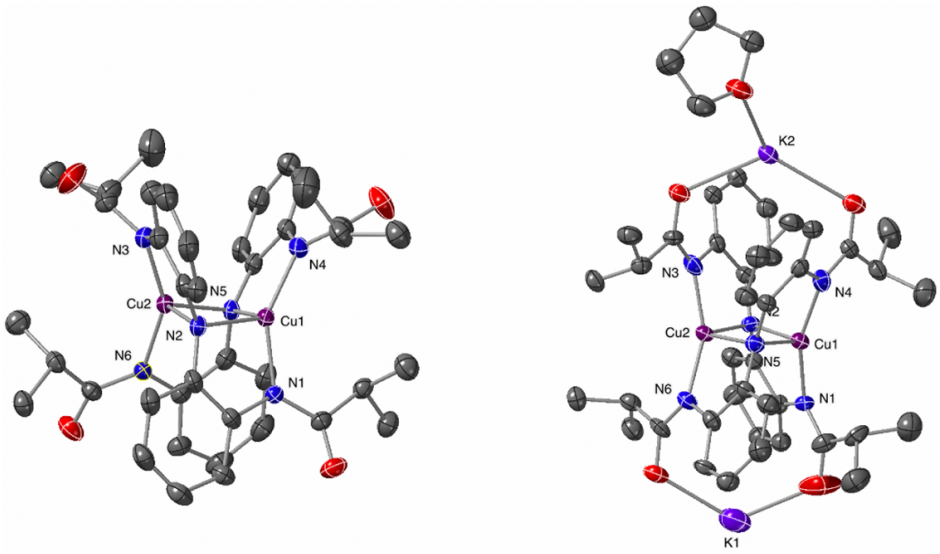

1^{2-} **2·THF**

Figure 2-2. Single-crystal structures of $\mathbf{1}^{2-}$ [5] and **2**·THF obtained from X-ray diffraction. 50% ellipsoid probility; counter-cations in $\mathbf{1}^{2-}$ and hydrogen atoms in both complexes are omitted for clarity.

Table 2-1. Selected bond angles of **1** and **2**·THF.

1	Bond Angle	**2**• THF	Bond Angle
N1–Cu1–N4	148.90˚	N1–Cu1–N4	157.78˚
N1–Cu1–N5	106.84˚	N1–Cu1–N5	112.39(5)˚
N2–Cu1–N4	124.12˚	N2–Cu1–N4	107.99˚
N2–Cu1–N5	104.29˚	N2–Cu1–N5	103.13˚
N2–Cu2–N5	104.29˚	N2–Cu2–N5	102.06˚
N3–Cu2–N6	148.90˚	N3–Cu2–N6	156.25˚
Cu1–N2–Cu2	74.76˚	Cu1–N2–Cu2	76.96˚
Cu1–N5–Cu2	74.76˚	Cu1–N5–Cu2	77.46˚

Table 2-2. Selected bond lengths of **1** and **2**·THF.

1	Bond length (Å)	**2**• THF	Bond length (Å)
N2–Cu1	2.097	N2–Cu1	2.091
N2–Cu2	2.123	N2–Cu2	2.118
N5–Cu1	2.123	N5–Cu1	2.092
N5–Cu2	2.097	N5–Cu2	2.095
Cu1–Cu2	2.562	Cu1–Cu2	2.619

Both complexes as well as their reactions with excess O_2 were also characterized with the UV-vis-NIR spectroscopy (the spectroscopic characterization of **1** was performed in previous studies[5]). As shown below in Figure 2-3, both **1** and **2** possess similar absorption features prior to O_2 addition,

with a major absorption feature in the near IR region at 960 nm. Two more absorption features in the visible light region that appear at 530 nm and 600 nm are not well separated from each other. A feature of lower intensity appears at 740 nm. Upon O_2 addition, the absorption in the near IR region extinguishes in both complexes. An increase in intensity of indistinguishable and broadened features in the 600-800 nm region is observed. A distinct peak in the UV region at around 330 nm is observed in both spectrum, with a shoulder of lower intensity at around 440 nm. These features in the lower wavelength region corresponds well with features in both the μ-η^2:η^2-peroxo and the bis(μ-oxo) type of the Cu_2O_2 cores (see Chapter 1). These results indicate that both complexes are active in the presence of O_2 and that a Cu_2O_2 core could be forming.

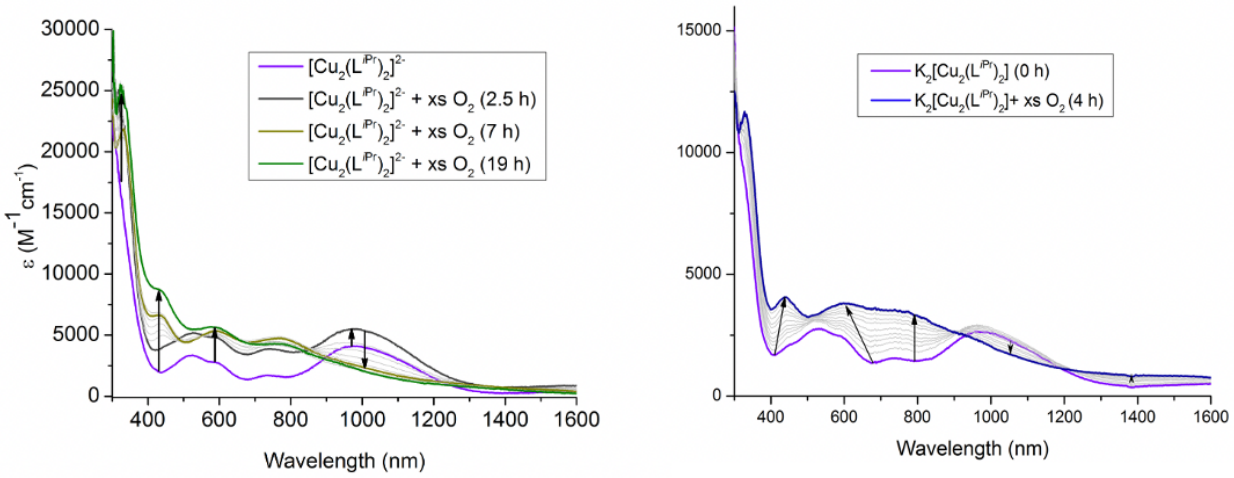

Figure 2-3. UV-vis-NIR absorption spectra at 25 ℃ of **1** reacting with excess O_2 in acetonitrile (left)[5], and **2** reacting with excess O_2 in acetonitrile (right).

Catalytic Aerobic Oxidation

To probe the catecholase activity of both **1** and **2**, they were both tested as catalysts for the aerobic oxidation of 3,5-di(tert-butyl)catechol (3,5-DTBC) under a constant flow of O_2. The 3,5-DTBC

and the catalyst were added to a solution of acetonitrile at 25 ℃ in an environment of N_2 before the reaction mixture was subject to O_2 addition. A detailed procedure is provided in the experimental section.

Both **1** and **2** displayed the best catalytic activity at 5 mol% of catalyst loading (Table 2-3, entries 1 and 2). After 0.5 hour of reaction, the starting material could no longer be detected by ^{1}H NMR, and 67% and 80% of the catechol were converted to the quinone product when **1** and **2** were used, respectively. The rest of the starting materials are believed to have been converted to other minor decomposition products that were not identifiable by ^{1}H NMR. Complex **2** continued to show better catalytic activity than **1** when the catalyst loading was decreased to 1 mol% and the reaction time increased to 4 h (entries 3 and 4). This difference in catalytic activity of **1** and **2** is also observed in the comparison of UV-vis-NIR spectra of the reactions using **1** and **2** as the catalyst (Figure 2-4): the absorption feature at 400 nm indicating quinone formation starts to appear in the reaction with **2** even before O_2 addition, showing that **2** is capable of oxidizing catechol in the absence of O_2. Whereas for **1**, O_2 is required for the oxidation to proceed. In addition, while the color change from dark purple to burgundy in reaction mixtures using **1** was observed after O_2 addition, this color change in the reaction using **2** could be observed before O_2 addition once catechol was added. The earlier color change in the reaction with **2** also indicates catechol oxidation without O_2.

The higher catalytic activity of **2** was no longer observed when the catalyst loading was further decreased to 0.5 mol% and to 0.1 mol%. At these much lower catalyst loading, **1** started to show greater catalytic activity than **2** even if the reaction time when using **2** was longer (entries 5-8).

Control reactions using CuI or $CuBr_2$ as the catalyst were also run, demonstrating that neither Cu(I) nor Cu(II) salts are capable of catalyzing the reaction and therefore, suggesting that the redox active ligand is required.

Table 2-3. Catalytic aerobic oxidation of 3,5-di(tert-butyl)catechol

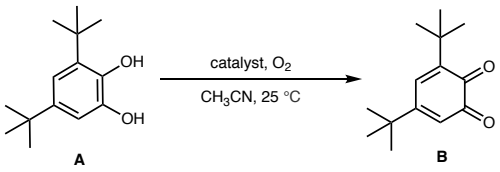

Entry	Catalyst	Catalyst Loading	Reaction Time (h)	[a]A%	[a]B%	[a]TON
1	**1**	5 mol%	0.5	0%	67%	13
2	**2**	5 mol%	0.5	0%	80%	15
3	**1**	1 mol%	4	68%	27%	27
4	**2**	1 mol%	4	38%	48%	45
5	**1**	0.5 mol%	20	46%	57%	107
6	**2**	0.5 mol%	24	40%	51%	100
7	**1**	0.1 mol%	44	79%	18%	163
8	**2**	0.1 mol%	45	75%	12%	116
9	CuI/$CuBr_2$	5 mol%	0.5	100%	0%	0

a. Yields and turnover numbers (TONs) are determined by ^{1}H NMR using 1,3,5-trimethoxybenzene as the internal standard.

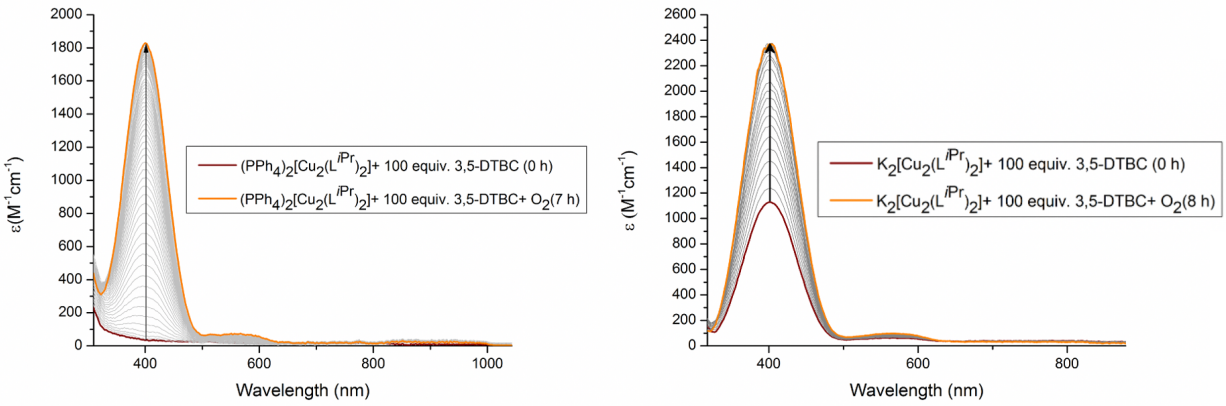

Figure 2-4. UV-vis-NIR absorption spectra of **1**(left) and **2**(right) reacting with 3,5-di(tert-butyl)catechol (3,5-DTBC) in acetonitrile at 25 °C before and after adding excess O_2.

Isolation of the off-pathway species $Cu_2(DTBSQ)_4$

The change in the relative catalytic activity of **1** and **2** at high and low catalyst loadings indicates that either product inhibition or catalyst deactivation could take place when **2** is used at lower catalyst loading. In a titration of **2** with different equivalents of 3,5-DTBC at 25 °C monitored by UV-vis-NIR absorption spectroscopy, the absorption features of **2** decreased as more 3,5-DTBC was added (Figure 2-5). These diminished absorption features together with the observed color change in the reaction mixture prior to O_2 addition together suggest that while **2** could oxidize 3,5-DTBC without O_2, it could also be inhibited by 3,5-DTBC at the same time, and an off-pathway species could be formed that renders the catalytic system unreactive.

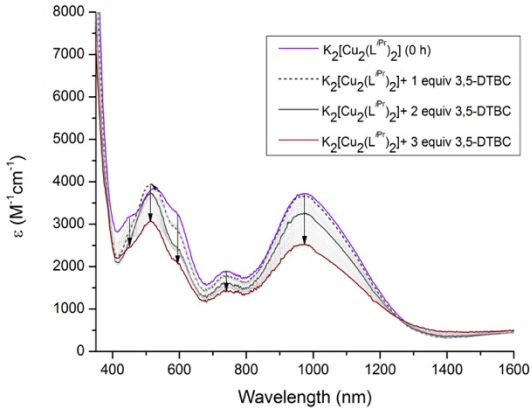

Figure 2-5. UV-vis-NIR absorption spectrum of titrating a solution of **2** in acetonitrile with different equivalents of 3,5-DTBC at 25 ℃.

In an effort to isolate the potential off-pathway species, **2** was reacted with 100 equivalents of 3,5-DTBC at 25 ℃ in an environment of N_2 (Scheme 2-3). The reaction mixture was dried and redissolved in hexane, resulting in a dark purple solution with a blue precipitate. The blue precipitate was filtered out and dried. A detailed procedure is provided in the experimental section.

Single-crystals suitable for X-ray diffraction were obtained by slow evaporation at low temperature in a concentrated solution of acetonitrile; the acetonitrile solution was green. The single crystals are of a binuclear Cu complex, $Cu_2(DTBSQ)_4$, which has four semiquinone ligands (Figure 2-6).

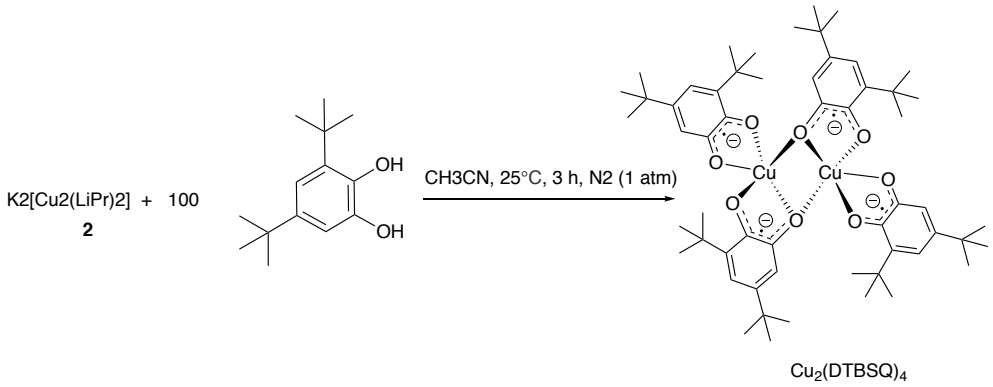

Scheme 2-3. The synthesis of $Cu_2(DTBSQ)_4$.

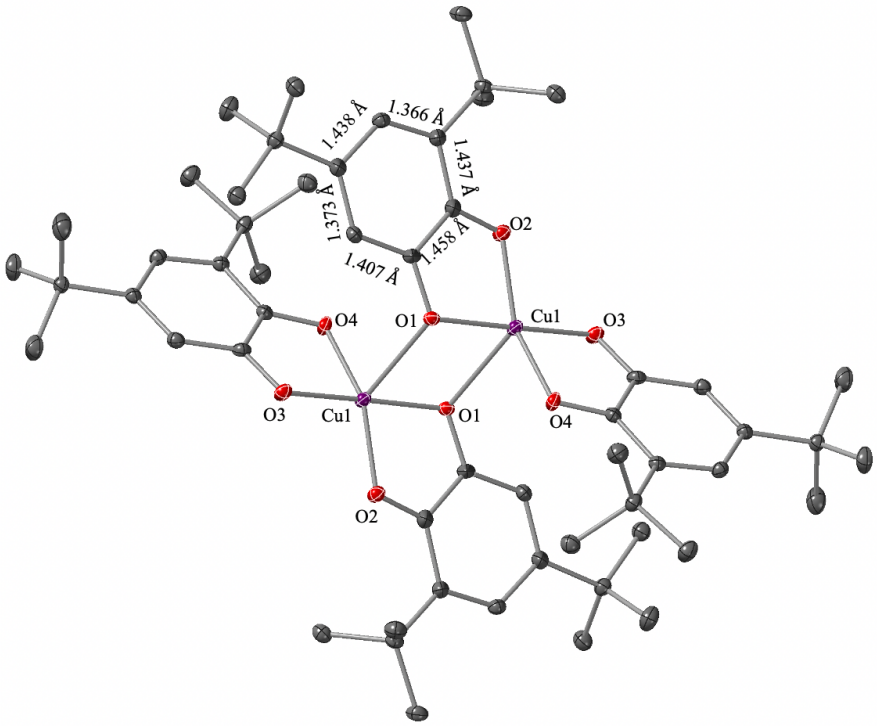

Figure 2-6. The single-crystal structure of $Cu_2(DTBSQ)_4$ with certain bond lengths labeled. (50% ellipsoid probability)

The semiquinone ligands in $Cu_2(DTBSQ)_4$ are the one-electron oxidized product of the 3,5-DTBC. Based on this structure and the limited reactivity in the presence of high concentrations of 3,5-DTBC we propose that **2** oxidizes 3,5-DTBC to 3,5-DTBSQ prior to O_2 addition and the semiquinones displace the original L^{iPr} ligands on **2**, forming the $Cu_2(DTBSQ)_4$ species. The lengths of the bonds on the semiquinone rings labeled in Figure 2-6 supports the assignment of this complex as a binuclear Cu(II) complex with semiquinone ligand radicals. Additional evidence of the existence of the ligand radicals is provided in the UV-vis-NIR absorption spectra of the complex that show broad absorption features in the NIR region, which are characteristic of organic ligand radicals (Figure 2-7). The spectra also indicate a dynamic equilibrium of semiquinone association and dissociation. At -30 ℃, the absorption features in the spectrum have higher molar absorptivity, indicating that the ligand dissociation is slowed down at such temperature. In order to confirm that $Cu_2(DTBSQ)_4$ was not catalytically relevant, it was tested as the catalyst for the aerobic oxidation of 3,5-DTBC at a 5 mol% catalyst loading. Only trace quinone was observed, which we propose were the dissociated semiquinone ligands that were further oxidized by O_2 to the quinone.

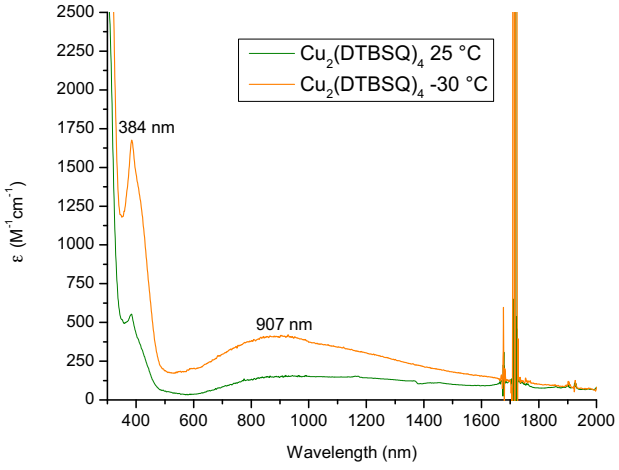

Figure 2-7. UV-vis-NIR absorption spectra of $Cu_2(DTBSQ)_4$ in acetonitrile taken at both 25 ℃ and at 30 ℃.

Conclusion

Binuclear Cu(II) complexes $(PPh_4)_2[Cu_2(L^{iPr})_2]$ (**1**) and $K_2[Cu_2(L^{iPr})_2]$ (**2**) have been synthesized. Complex **2** has been characterized by single-crystal X-ray diffraction and UV-vis-NIR spectroscopy, and the results have been compared with those of **1** obtained from previous research.[5] In the single-crystal structure of **2**, both K^+ counter-cations are coordinated to the ligand backbone, creating a second coordination sphere that is not present in **1**. This coordination of the counter-cation changes the geometry of **2** and reduces its level of symmetry. Both complexes were tested as catalyst for the oxidation of 3,5-di(tert-butyl)catechol(3,5-DTBC) using O_2 as the terminal oxidant, and it was demonstrated that the counter-cations do have an impact on the catalytic activity of the complex. The best yield (80%) was achieved when 5 mol% of **2** was used for the reaction in acetonitrile at 25 ℃ with a constant flow of oxygen. Complex **2** showed better catalytic activity than **1** at higher catalyst loadings (5 mol% and 1 mol%). However, this advantage diminished when the loading was reduced to below 0.5 mol% because an off-pathway species $Cu_2(DTBSQ)_4$ was formed in the reaction using **2**. $Cu_2(DTBSQ)_4$ was formed because **2** is capable of oxidizing 3,5-DTBC to quinone without the addition of O_2, but while the oxidation takes place, the one-electron oxidized semiquinones can displace the L^{iPr} ligands on **2**, forming the catalytically inactive $Cu_2(DTBSQ)_4$. This ligand displacement was more significant at higher concentrations of 3,5-DTBC, and this explains the diminished catalytic activity of **2** at lower catalyst loading. To prevent this ligand displacement that results in catalyst deactivation, future studies will focus on changing the substituents on the amides of the ligand backbone to determine how altered electronic and steric environments affect catalytic activity.

Experimental section

General considerations and materials

All manipulations that require an environment without O_2 and H_2O are conducted in an MBraun Labmaster 130 drybox filled with a N_2 atmosphere. All reagents used were purchased from commercial vendors, and all anhydrous solvents were purchased from Sigma-Aldrich. ^{1}H NMR spectra were taken on INOVA and Bruker 400 MHz spectrometers operating in the pulse Fourier transform mode at ambient temperature. Chemical shifts are referenced to residual solvent. UV-vis-NIR absorption spectra were taken on a Shimadzu UV 3600 spectrophotometer using 1.0 cm quartz cuvettes. X-ray diffraction studies were carried out in the X-ray Crystallohraphy Laboratory at Emory Uiversity on a XtaLAB Synergy diffractometer. Single crystals suitable for X-ray diffraction were mounted on a loop with Paratone® oil, and data were collected using XtaLAB Synergy diffractometer equipped with an Oxford Cryosystems low-temperature device, operating at T = 100(2) K. Data were measured using ω scans of 0.5° per frame for 30.0 s using MoK_α radiation (micro-focus sealed X-ray tube, 50 kV, 1.0 mA).

Ligand synthesis

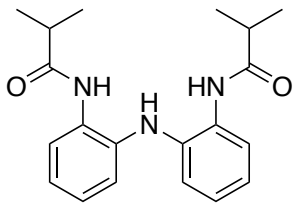

H_3L^{iPr}

2,2'-Bis(isopropylacetoamido)diphenylamine [HN(*o*-PhNHC(O)*i*Pr)$_2$] (H_3L^{iPr}): In a 500 mL round bottom flask, 2-nitroaniline (0.6907g, 0.005 mol) and 1-fluoro-2-nitrobenzene (0.7055g, 0.005 mol) were added and stirred in dimethyl sulfoxide (DMSO) for 15 min. Potassium tert-

butoxide (1.1221g, 0.01 mol) was then slowly added to the reaction mixture. The reaction was stirred for 24 hours and then quenched by adding enough deionized water, so that all the formed bis(2-nitrophenyl)amine formed could precipitate from the solution as orange solids, which was isolated by filtration through a fritted glass filter. The orange product was washed with deionized water and *n*-hexanes and dried under vacuum. The dried orange powder was then transferred to a Parr® pressure tested hydrogenation vessel and dissolved in 30 mL of THF, and 10 wt% of Pd/C was added to the vessel. The reaction mixture was hydrogenated under H_2 (50 psi) for 30 min, followed by a quick filtration through Celite®. The filtrate was collected and concentrated under reduced pressure to yield light orange oil, to which *n*-hexanes were added. The oil and *n*-hexanes were let stirring for 3 hours and off-white solids of bis(aminophenyl)amine could be obtained, which were dried under vacuum. The dried powder was weighed and added to a 250 mL round bottom flask and let stirring in dichloromethane. To this flask, 2 equivalents of triethylamine was adde, and the reaction was stirred in an ice bath for 20 min. Afterwards, 2 equivalents of isobutyryl chloride was then slowly added to the reaction mixture, which was stirred for 24 hours and allowed to slowly return to room temperature. Extraction of the reaction mixture was then performed first with saturated aqueous sodium bicarbonate solution for three times, and then with brine solution. The organic layer was collected, dried over $MgSO_4$, filtered, and then dried to solid using a rotary evaporator. The solid was then stirred in *n*-hexanes for 3 hours, filtered, and dried under reduced pressure to obtain the final product H_3L^{iPr}, which was an off-white powder. **^{1}H NMR** (400 MHz, $CDCl_3$): δ 7.71 (s, 2H), 7.69 (dd, J = 7.8, 1.7 Hz, 2H), 7.05 (td, J = 7.6, 1.7 Hz, 2H), 7.00 (td, J = 7.6, 1.7 Hz, 2H), 6.87 (dd, J = 7.8, 1.6 Hz, 2H), 5.71 (s, 2H), 2.56 (septet, J = 6.9 Hz, 2H), 1.15 (d, J = 6.9 Hz, 12H).

Complex syntheses

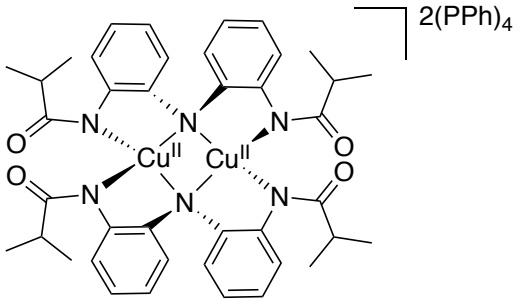

$(PPh_4)_2[Cu_2(L^{iPr})_2]$

$(PPh_4)_2[Cu_2(N(o\text{-}PhNC(O)iPr)_2)_2]$ ($(PPh_4)_2[Cu_2(L^{iPr})_2]$): In a 20 mL vial in the glovebox, H_3L^{iPr} (33.94 mg, 0.1 mmol) and KH (12.43 mg, 0.31 mmol) were added to a solution of anhydrous dimethylformamide. The reaction was let stirring for 30 min until no bubbles of H_2 could be observed. $CuBr_2$ (22.34 mg, 0.1 mmol) and PPh_4Br (41.93 mg, 0,1 mmol) were then added at the same time. The reaction was stirred for 24 hours, and then DMF was removed under reduced pressure. The dried sample was redissolved in anhydrous acetonitrile to precipitate KBr. After filtering the sample through fritted glass filter, the filtrate was collected and dried under reduced pressure. Anhydrous *n*-hexanes were added to the dried sample, and it was stirred for 3 hours. Dark purple powder formed in the solution, which was filtered, washed with *n*-hexanes, and dried under reduced pressure to obtain the final product. X-ray quality crystals of $(PPh_4)_2[Cu_2(L^{iPr})_2]$ were obtained by diffusing diethyl ether into a concentrated solution in acetonitrile.[5] Crystallographic data are provided in Table 2-4.[5]

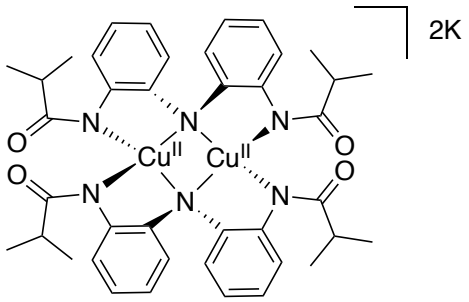

$K_2[Cu_2(L^{iPr})_2]$

($K_2[Cu_2(N(o\text{-}PhNC(O)iPr)_2)_2]$ ($K_2[Cu_2(L^{iPr})_2]$): In a 20 mL vial in the glovebox, H_3L^{iPr} (33.94 mg, 0.1 mmol) and KH (12.43 mg, 0.31 mmol) were added to a solution of anhydrous dimethylformamide. The reaction was let stirring for 30 min until no bubbles of H_2 could be observed. $CuBr_2$ (22.34 mg, 0.1 mmol) was then added at the same time. The reaction was stirred for 24 hours, and then DMF was removed under reduced pressure. The dried sample was redissolved in anhydrous acetonitrile to precipitate KBr. After filtering the sample through fritted glass filter, the filtrate was collected and dried under reduced pressure. Anhydrous *n*-hexanes were added to the dried sample, and it was stirred for 3 hours. Dark purple powder formed in the solution, which was filtered, washed with *n*-hexanes, and dried under reduced pressure to obtain the final product. X-ray quality crystals of $K_2[Cu^{II}_2(L^{iPr})_2]$ were obtained by diffusing diethyl ether into a concentrated solution in THF. Crystallographic data are provided in Table 2-5.

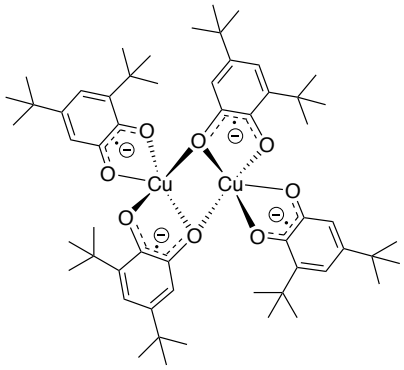

$Cu_2(DTBSQ)_4$

$Cu_2(((CH_3)_3C)_2C_6H_2\text{-}1,2\text{-}O_2)_4$ ($Cu_2(DTBSQ)_4$): In a 20 mL vial in the glove box, $K_2[Cu_2(L^{iPr})_2]$ (17.52 mg, 0.02 mmol) and 100 equivalents of 3,5-di(tert-butyl)catechol (44.46 mg, 0.2 mmol) were added in a solution of anhydrous acetonitrile and stirred for 3 hours. The acetonitrile solvent was then removed under reduced vacuum, and the dried sample was redissolved in *n*-hexanes. Blue precipitates formed in *n*-hexanes was filtered out from the dark purple solution with a fritted glass filter, washed with *n*-hexanes, and dried under reduced pressure. X-ray quality crystals were obtained by dissolving the blue solid in acetonitrile and setting up a slow evaporation in the freezer.

Catalytic aerobic oxidation of 3,5-di(tert-butyl)catechol: To a 50 mL round botton flask in the glovebox, complex **1** or **2** of different catalyst loadings (5 mol%, 1 mol%, 0.5 mol%, 0.1 mol%) were dissolved in anhydrous acetonitrile with the corresponding equivalents of 3,5-di(tert-butyl)catechol. 3 Å molecular sieves of 50 mg were also added to the solution. The round bottom flask was sealed with a septum and electrical tape before it was taken out of the glove box. Then, a constant flow of O_2 was introduced to the round bottom flask with a needle submerged in the reaction mixture. The reaction was stirred at 25 ℃ for the duration of the reaction times. Afterwards, 1,3,5-trimethoxybenzene was added immediately to the mixture as a standard for ^1H NMR, and the mixture was dried under reduced pressure. The mixture was then dissolved in ethyl

acetate, and an acid workup was performed by extracting the ethyl acetate solution with 1M HCl aqueous solution for three times. The organic layer that contained was collected and dried under reduced pressure to obtain a dark brown oil. ^{1}H NMR of the crude reaction mixture containing the starting material, the product, and the standard was taken to determine the yield. The spectrum contains shifts corresponding to the 2,4-di(tert-butyl)quinone final product. **^{1}H NMR (400 MHz, $CDCl_3$):** δ 6.91 (s, 1H), 6.19 (s, 1H), 1.25 (s, 9H), 1.20 (s, 9H).

Table 2-4. Crystallographic data for **1**.[5]

	1
Empirical formula	$C_{89}H_{85.5}Cu_2N_{6.5}O_4P_2$
Formula weight	1499.16
T (K)	173(2)
λ (Å)	0.71073
Crystal size (mm^3)	0.46 x 0.19 x 0.14
Crystal system	Orthorhombic
Space group	$C222_1$
a (Å)	13.587(3)
b (Å)	22.642(5)
c (Å)	25.303(5)
α (º)	90
β (º)	90
γ (º)	90
V ($Å^3$)	7790(3)
Z	4
ρ_{calcd} (g/cm^3)	1.278
GOF on F^2	1.046
*R*1, *wR*2 [$I > 2\alpha(I)$]	0.0459, 0.1075

Table 2-5. Crystallographic data for complexes **2**.

	2
Empirical formula	$C_{88}H_{104}Cu_4K_4N_{12}O_{10}$
Formula weight	1900.39
T (K)	103
λ (Å)	1.54184
Crystal size (mm^3)	0.30 x 0.1 x 0.15
Crystal system	Monoclinic
Space group	$P2_1/c$
a (Å)	11.8176
b (Å)	12.3995
c (Å)	34.6563
α (º)	90
β (º)	99.744
γ (º)	90
V ($Å^3$)	5005.0
Z	2
δ_{calc} (g/m^3)	1.261
GOF on F^2	1.466
*R*1, *wR*2 [$I > 2\alpha(I)$]	0.1005, 0.3192

References

1. Collins, T. J. *Acc. Chem. Res.* **1994**, *27*, 279-285.

2. Sharma, S. K.; May, P. S.; Jones, M. B.; Lense, S.; Hardcastle, K. I.; MacBeth, C. E. *Chem. Commun.* **2011**, *47*, 1827-1829.

3. Villanueva, O.; Weldy, N. M.; Blakey, S. B.; MacBeth, C. E. *Chem. Sci.* **2015**, *6*, 6672-6675.

4. Corcos, A. R.; Villanueva, O.; Walroth, R. C.; Sharma, S. K.; Bacsa, J.; Lancaster, K. M.; MacBeth, C. E.; Berry, J. F. *J. Am. Chem. Soc.* **2016**, *138*, 1796-1799.

5. Liu, E. E. L.-N. Emory University, Atlanta, GA. Unpublished work, 2019.

6. Yang, L.; Powell, D. R.; Houser, R. P. *Dalton Trans.* **2007**, *955-964*.

Chapter 3. The Isolation and Characterization of Two Hydroxo-Bridged Cu Complexes and One Cu-Phenolate Complex

Introduction

The incorporation of sterically demanding substituents on ligand backbones of transition metal complexes often leads to the formation of coordinatively unsaturated complexes. Those bulky ligands can hinder the metal center from coordinating to other ligands. Some examples of coordinatively unsaturated complexes with bulky ligands are shown below (Figure 3-1). In these cases, the incorporation of multiple ring structures and branched alkyl groups increases the steric hindrance. To explore the effect of similar structural motifs in the bis(amidophenyl)amine type ligands, two sterically encumbered ligands with trimethylphenyl and triisopropylphenyl substituents (H_3L^{TMP} and H_3L^{TRIP}) were designed and synthesized. This ligands were then used to coordinate to Cu(II) centers. It was proposed that these bulky substituents would prevent the formation of binuclear complexes of the $[Cu_2L_2]^{2-}$ type with bridging N atoms (L = Ligand, see chapter 2 for examples), and a mononuclear complex of the $[CuL]^-$ will form. While the predicted mononuclear complex was not formed, some unexpected Cu complexes with bridging-hydroxo and phenolate ligands were isolated. In this chapter, the characterizations of these complexes are reported.

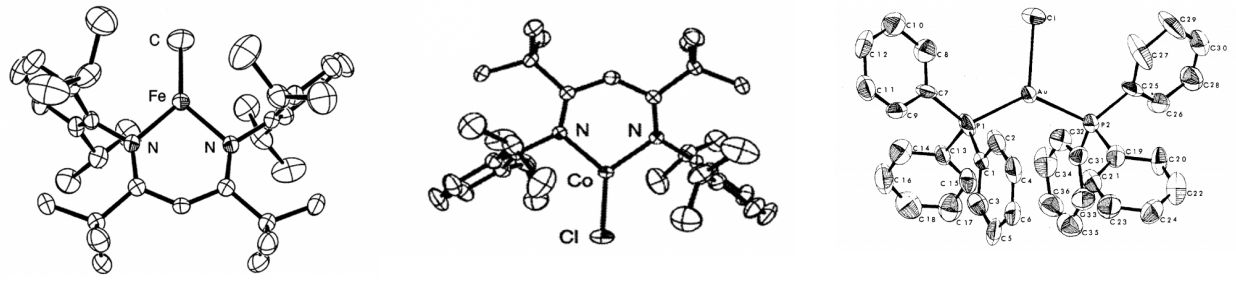

Figure 3-1. Examples of coordinatively unsaturated complexes with bulky ligands.[1, 2]

Results and Discussion

Ligand syntheses

Ligands H_3L^{TMP} and H_3L^{TRIP} were synthesized based on a modified version of a previously reported procedure (Scheme 3-1).[3] The synthesis of the bis(aminophenyl)amine precursor followed the same procedure as described in chapter 2. A final acyl transfer between the bis(aminophenyl)amine with 2,4,6-trimethylbenzoyl chloride or 2,4,6-triisopropylbenzoyl chloride yielded the ligands H_3L^{TMP} and H_3L^{TRIP} respectively. A detailed procedure is provided in the experimental section.

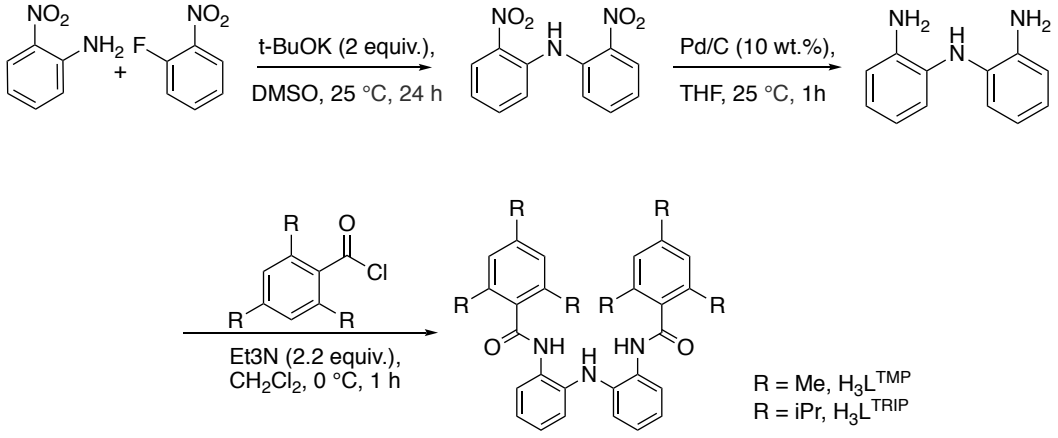

Scheme 3-1. The syntheses of ligands H_3L^{TMP} and H_3L^{TRIP}.

Isolation and characterization of $K_2[Cu_3(L^{TMP})_2(OH)_2]$

In an attempt to synthesize complex **3**, the ligand H_3L^{TMP} was deprotonated by three equivalents of KH, which was followed by the addition of one equivalent of $CuBr_2$ (Scheme 3-2). The reaction yielded a complex mixture. First, a grey-green colored powder was obtained after removing the solvent, stirring the product in *n*-hexanes, and filtering out the precipitated product. A detailed procedure is provided in the experimental section. However, diffraction quality crystals could not be obtained from this powder. The ^1H NMR of the grey-green powder was not

diagnostic, with broadened peaks due to the paramagnetic Cu(II) center. The only data that suggests that **3** is from is the mass spectrum, which contained a signal at m/z = 551.1651 in the negative ion mode corresponding to $[Cu(II)(L^{TMP})]^-$. However, since fragmentation can occur upon electron ionization in the mass spectrometer. Therefore, the result is not definitive.

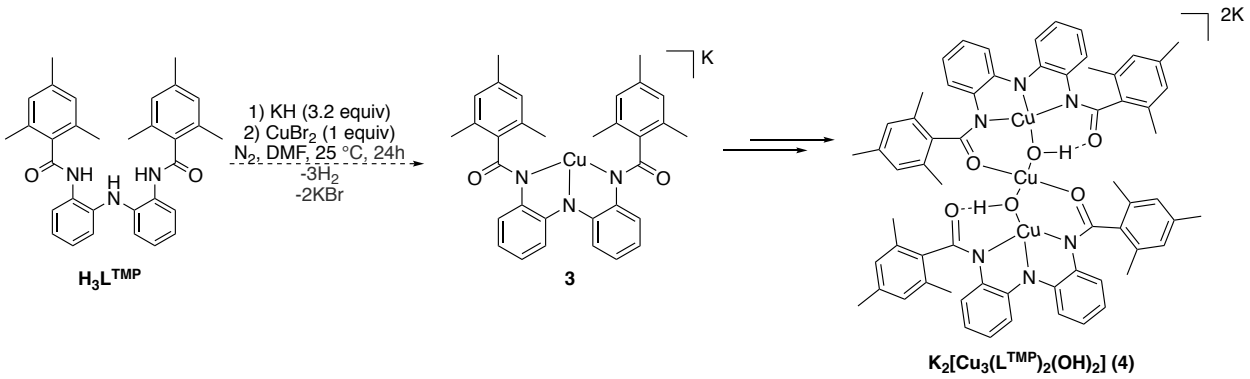

Scheme 3-2. The isolation of $K_2[Cu_3(L^{TMP})_2(OH)_2]$ (**4)** from the attempted synthesis of **3**.

Dark orange crystals were obtained from the slow evaporation of the reaction mixture at low temperature over three weeks. The solid-state structure was determined to be $K_2[Cu^{II}_3(L^{TMP})_2(OH)_2]$ (**4**) by X-ray crystallography (Figure 3-2). The hydroxide groups in **4** could result from trace H_2O or O_2 contamination in the environment of the glovebox. The ligand could be deprotonated, and the resulting OH^- could then displace the ligand to coordinate to the Cu center. Selected bond lengths and bond angles of the single crystal of **4** are displayed in Table 3-1. The crystal of **4** is centrosymmetric. Cu1 is coordinated to four oxygen atoms, two from the hydroxides and the other two from the amido carbonyls of the ligand backbone. This Cu center is square planar, with a τ_4 value of 0. The other two Cu centers have a distorted square planar geometry, each with a τ_4 value of 0.11. The hydrogen atoms on the two hydroxides form H-bonding interactions with the amido oxygen on the ligand backbone to stabilize the structure.

The two K^+ counter-cations are also coordinated each to three oxygen atoms and three solvent molecules to further stabilize the structure.

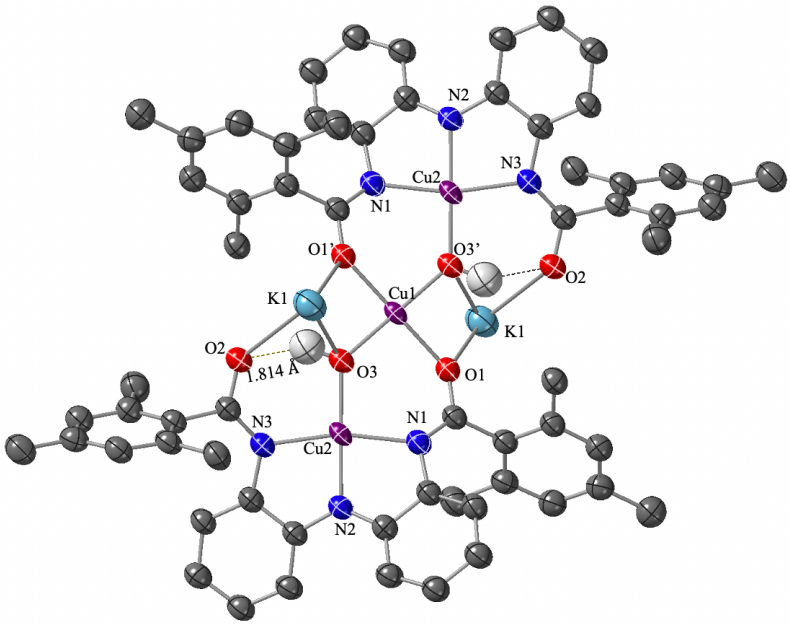

Figure 3-2. The single-crystal structure of **4** (50% ellipsoid probability). Coordinating solvent molecules and hydrogen atoms not involved in hydrogen-bonding interactions are omitted for clarity.

Table 3-1. Selected bond lengths and bond angles of **4**.

Bond	Bond length (Å)	Bond angle	Bond angle
Cu1–O1	1.987	O1–Cu1–O1’	180.00 °
Cu3–O3	1.866	O3–Cu1–O3’	180.00 °
Cu2–N1	2.011	O1–Cu–O3	93.07 °
Cu2–N2	1.881	N1–Cu2–N2	82.85 °
Cu3–N3	2.014	N1–Cu2–N3	165.73 °
Cu2–O3	1.872	O3–Cu2–N2	179.19 °

In an effort to find a reproducible route to synthesize **4**, a procedure involving adding KOH as the source of the hydroxide ligands was attempted (Scheme 3-2.) After the work-up, the grey-green powder was isolated and crystals suitable for X-ray diffraction were obtained through slow evaporation from diethyl ether. A detailed procedure is provided in the experimental section.

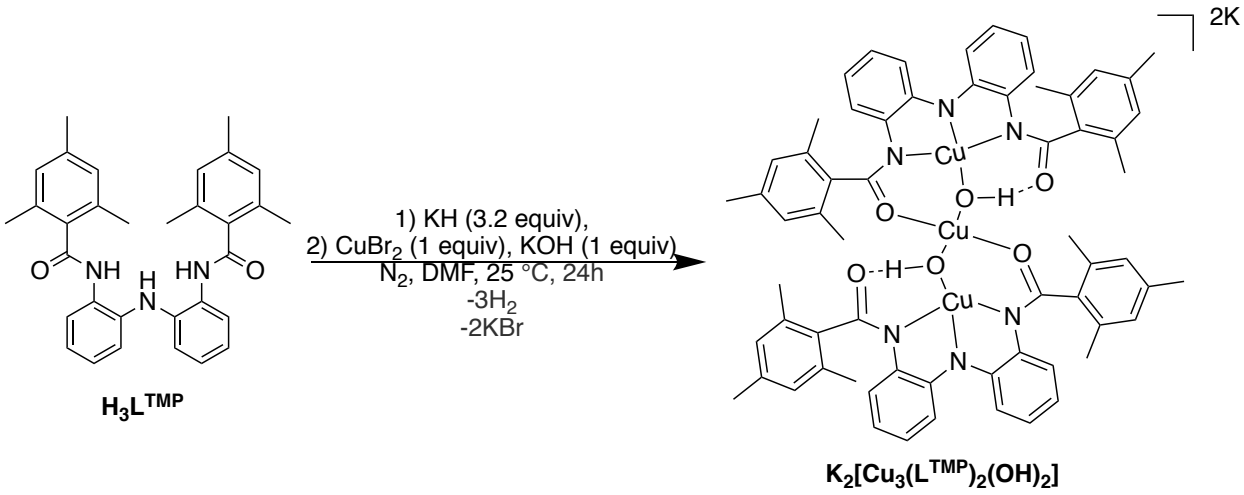

Scheme 3-2. Synthesis of **4** by adding KOH.

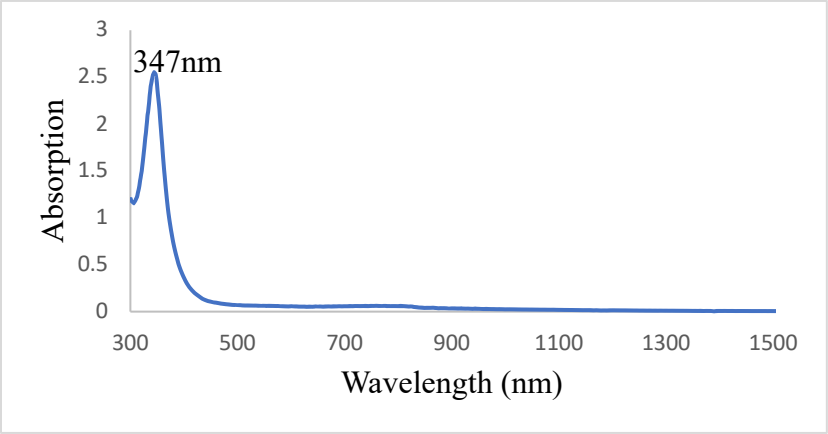

Figure 3-3. UV-vis-NIR spectrum of **4** in acetonitrile at 25 °C.

The single-crystal structure confirmed the successful synthesis of **4** as the same structure as the previous time was obtained, with the exception that the coordinating solvent was diethyl ether instead of acetonitrile. Some of the crystals were then dissolved in anhydrous acetonitrile, and a UV-vis-NIR spectrum was obtained (Figure 3-3). The complex had a distinct absorption feature at 347 nm and a broad absorption feature of very low intensity in the 500-800 nm region. A modified method of adding the H_3L^{TMP} ligand, KH, $CuBr_2$, and KOH in the exact 2:6:3:2 ratio as the ratio in **4** is currently being tested to confirm whether **4** could also be successfully obtained. The inability to isolate **3** and the unexpected synthesis of **4** together suggest that the mononuclear Cu complex with one coordinating L^{TMP} ligand is unstable, and another ligand is required to occupy the fourth coordination site. However, due to the large steric hindrance from the trimethylphenyl substituents, the $[Cu_2L_2]^{2-}$ type structure could not be formed either. Thus, **4** is preferentially formed, which uses the small μ-hydroxo ligand to occupy the vacant site and stabilize the structure.

Isolation and characterization of $K[Cu(L^{TRIP})(OPh)]$ and $K[Cu_2(OH)(L^{TRIP})_2]$

Following the same general procedure as in the attempted synthesis of **3**, H_3L^{TRIP} was deprotonated and treated with $CuBr_2$ (Scheme 3-2). From the unfiltered acetonitrile solution, dark crystals of **6** suitable for X-ray diffraction were obtained through slow evaporation from acetonitrile at room temperature. The filtrate was dried and stirred in *n*-hexanes to obtain dark purple powder, and then dissolved in acetonitrile. Slow evaporation at -33 ℃ yielded dark crystals of **7** that were suitable for X-ray diffraction. The isolation of complex **5** was unsuccessful, and its formation in solution is only supported by a signal at m/z = 719.353 in the negative ion mode mass spectrum, which corresponds to $[Cu(II)(L^{TRIP})]^-$. Complexes **6** and **7**

could have been formed because of trace O_2 and H_2O in the environment of the glovebox. O_2 could have activated the C-C bond on the ligand bone, forming the phenolate that coordinates to Cu in **6**. Complex **7** could have been formed when the trace amount of H_2O was deprotonated by the redox-active ligand backbone and then became a bridging ligand.

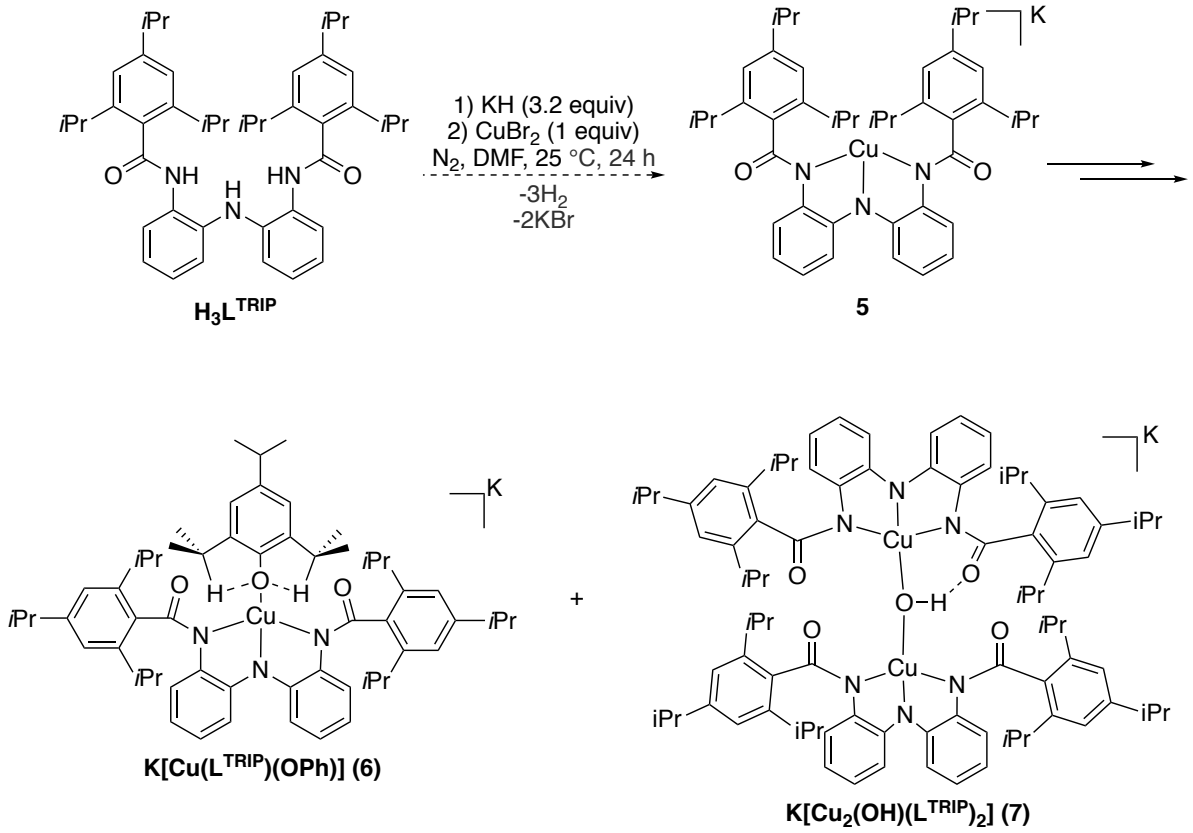

Scheme 3-3. The isolation of K[Cu(L^{TRIP})(OPh)] (**6**) and K[Cu_2(OH)(L^{TRIP})] (**7**) from the attempted synthesis of **5**.

The single-crystal structures of **6** and **7** are shown in Figure 3-4. Selected bond lengths and bond angles are displayed in Table 3-2 and Table 3-3. Complex **6** has a Cu center in a slightly distorted seesaw geometry, with a τ_4 value of 0.49 calculated based on the bond angles. The two hydrogens of the isopropyl groups on the ortho positions of the phenolate forms weak hydrogen bonding interaction with the phenolate oxygen, with a bond length of 2.378 Å. The two Cu

centers in complex **7** are asymmetric from each other. The Cu1 center has a distorted seesaw geometry (τ_4 = 0.42) and the Cu2 center has a geometry between a square plane and a seesaw, with a τ_4 value of 0.35. The bridging hydroxo ligand is slightly closer to Cu1 as shown in the table of selected bond lengths. The hydrogen atom on the hydroxo ligand also forms a strong hydrogen bonding interaction with the ligand backbone of the Cu1 center, with a bond length of 1.894 Å. Rigidity of the structure is also improved with the K^+ counter-cation that coordinates to three of the oxygen atoms on the ligand backbone.

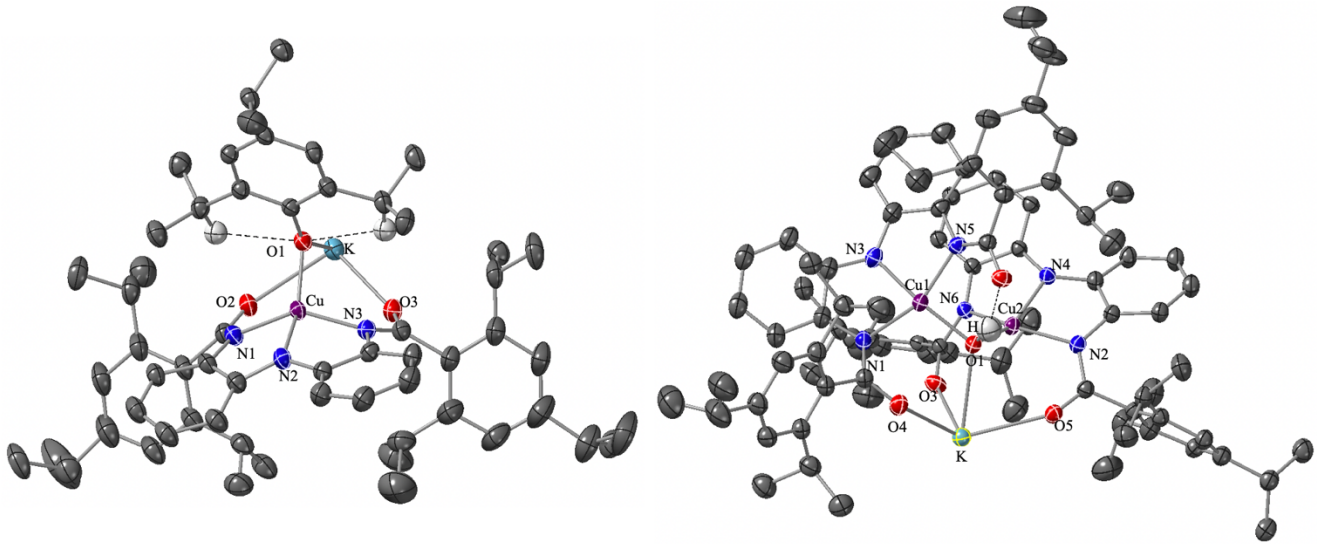

Figure 3-4. Single-crystal structures of **6** (left) and **7** (right) (50% ellipsoid probability). H-atoms not involved in hydrogen-bonding are omitted; coordinating acetonitrile solvent molecules in **7** are omitted for clarity.

Table 3-2. Selected bond lengths of **6** and **7**.

6	Bond length (Å)	**7**	Bond length (Å)
Cu–O1	1.907	Cu1–O1	1.912
Cu–N1	1.976	Cu2–O1	1.904
Cu–N2	1.936	Cu1–N3	1.930
Cu–N3	1.54	Cu2–C4	1.986
O1–H1	2.378	O2–H	1.894

Table 3-3. Selected bond angles of **6** and **7**.

6	Bond angle	**7**	Bond angle
N1–Cu–N3	143.85 °	N1–Cu1–N5	149.31 °
N2–Cu–O1	147.32 °	N2–Cu2–N6	151.15 °
N1–Cu–N2	82.58 °	N3–Cu1–O1	161.96 °
N3–Cu–N2	81.54 °	N4–Cu2–O1	149.06 °
N1–Cu–O1	106.52 °	Cu1–O1–Cu2	105.62 °

UV-vis-NIR spectra of complexes **6** and **7** in anhydrous acetonitrile were both taken (Figure 3-5 and Figure 3-6). Complex **6** has an absorption feature at 726 nm. Complex **7** has one absorption feature of high intensity at 345 nm, and two of lower intensities at 908 nm, and 985 nm. Complex **4** has a similar feature at 347 nm, and similar features in the 300-350 nm region have also been previously reported for Cu complexes with μ-hydroxo ligands and have been assigned as the hydroxo to Cu LMCT.[4] Based on this, we preliminarily assign here both the feature at 347 nm for complex **4** and the feature at 345 nm for complex **7** as the hydroxo to Cu LMCT.

Both complexes **6** and **7** are neutral with only one K^+ counter-cation, and therefore, the Cu centers in these complexes are assigned with a formal oxidation state of Cu(III). However, more evidence is required to confirm this assignment because the existence of Cu(III) is debated (see Chapter 1), and because it is possible that ligand radicals exist in these complexes. Attempts to obtain **6** and **7** in a higher yield and more reproducible manner are currently underway.

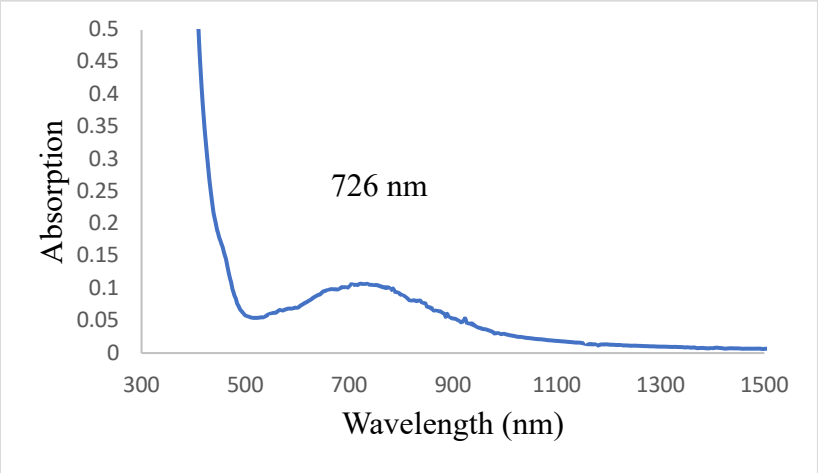

Figure 3-5. UV-vis-NIR spectrum of complex **6** in acetonitrile at 25 ℃.

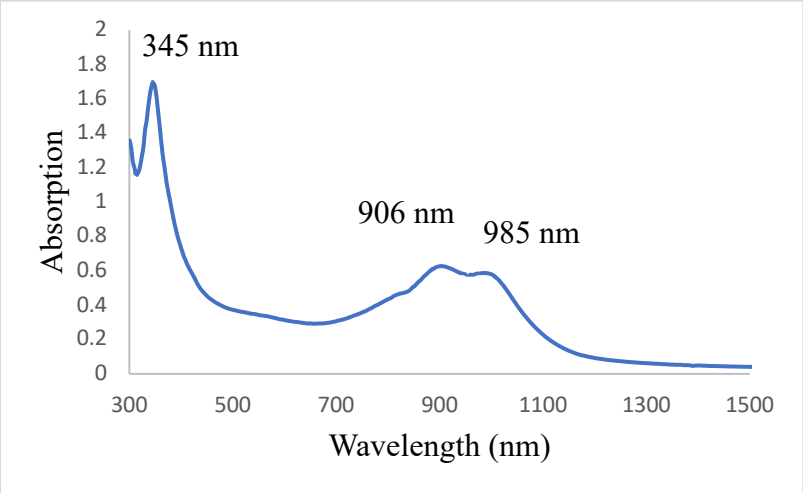

Figure 3-6. UV-vis-NIR spectrum of complex **7** in acetonitrile at 25 ℃.

Conclusion

Two hydroxo-bridged binuclear Cu complexes $K_2[Cu_3(L^{TMP})_2(OH)_2]$ (**4**) and $K[Cu_2(OH)(L^{TRIP})]$ (**7**), and a phenolate coordinated mononuclear Cu complex $K[Cu(L^{TRIP})(OPh)]$ (**6**) were unexpectedly isolated in the attempts to synthesize mononuclear Cu complexes supported by L^{TMP} and L^{TRIP} ligands. The incorporation of bridging-hydroxo ligands in both complexes **4** and

7 suggests that the desired mononuclear Cu complexes are relatively unstable likely because they are coordinatively unsaturated. Because of this, multimetallic complexes with smaller bridging-ligands such as the hydroxo ligands are formed. The isolation of the phenolate coordinated complex **6** reveals that a C–C bond cleavage of the ligand backbone can occur, possibly facilitated by the presence of O_2, forming the phenolate that is then coordinated to the Cu center. Isolation and characterization of these complexes, investigations of the oxidation states of the Cu centers in complexes **6** and **7**, and the oxidative chemistry of complexes **4, 6,** and **7** will be further studied.

Experimental section

General considerations and materials

All manipulations that require an environment without O_2 and H_2O are conducted in an MBraun Labmaster 130 drybox filled with a N_2 atmosphere. All reagents used were purchased from commercial vendors, and all anhydrous solvents were purchased from Sigma-Aldrich. ^{1}H NMR spectra were taken on INOVA and Bruker 400 MHz spectrometers operating in the pulse Fourier transform mode at ambient temperature. Chemical shifts are referenced to residual solvent. UV-vis-NIR absorption spectra were taken on a Shimadzu UV 3600 spectrophotometer using 1.0 cm quartz cuvettes. Mass Spectrometry was performed by the Mass Spectrometry Facility at Emory University on a Thermo LTQ-FTMS. X-ray diffraction studies were carried out in the X-ray Crystallohraphy Laboratory at Emory Uiversity on a XtaLAB Synergy diffractometer. Single crystals suitable for X-ray diffraction were mounted on a loop with Paratone® oil, and data was collected using XtaLAB Synergy diffractometer equipped with an Oxford Cryosystems low-temperature device, operating at T = 100(2) K. Data were measured using *w* scans of 0.5° per frame for 30.0 s using MoK_a radiation (micro-focus sealed X-ray tube, 50 kV, 1.0 mA).

Ligand syntheses

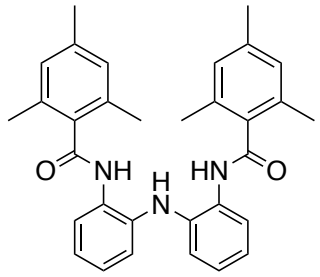

H_3L^{TMP}

2,2'-Bis(1,3,5-trimethylphenylacetoamido)diphenylamine [HN(*o*-PhNHC(O) (Ph(CH$_3$)$_3$))$_2$] (H_3L^{TMP}) : In a 500 mL round bottom flask, 2-nitroaniline (0.6907g, 0.005 mol) and 1-fluoro-2-

nitrobenzene (0.7055g, 0.005 mol) were added and stirred in dimethyl sulfoxide (DMSO) for 15 min. Potassium tert-butoxide (1.1221g, 0.010 mol) was then slowly added to the reaction mixture. The reaction was stirred for 24 hours and then quenched by adding enough deionized water, so that all the formed bis(2-nitrophenyl)amine formed could precipitate from the solution as orange solids, which was isolated by filtration through a fritted glass filter. The orange product was washed with deionized water and *n*-hexanes and dried under vacuum. The dried orange powder was then transferred to a Parr® pressure tested hydrogenation vessel and dissolved in 30 mL of THF, and 10 wt% of Pd/C was added to the vessel. The reaction mixture was hydrogenated under H_2 (50 psi) for 30 min, followed by a quick filtration through Celite®. The filtrate was collected and concentrated under reduced pressure to yield light orange oil, to which *n*-hexanes were added. The oil and *n*-hexanes were let stirring for 3 hours and off-white solids of bis(aminophenyl)amine could be obtained, which were dried under vacuum. The dried powder was weighed and added to a 250 mL round bottom flask and let stirring in dichloromethane. To this flask, 2 equivalents of triethylamine was added, and the reaction was stirred in an ice bath for 20 min. 2 equivalents of 1,3,5-trimethylbenzoyl chloride was then slowly added to the reaction mixture, which was stirred for 24 hours and allowed to slowly return to room temperature. Extraction of the reaction mixture was then performed first with saturated aqueous sodium bicarbonate solution for three times, and then with brine solution. The organic layer was collected, dried over $MgSO_4$, filtered, and then dried to solid using a rotary evaporator. The solid was then stirred in *n*-hexanes for 3 hours, filtered, and dried under reduced pressure to obtain the final product H_3L^{TMP}, which was an off-white powder. **^{1}H NMR** (400 MHz, $CDCl_3$): δ 7.81 (dd, J = 7.6, 1.9 Hz, 2H), 7.76 (s, 2H), 7.15-7.05 (m, 4H), 6.94 (dd, J = 7.4, 1.8 Hz), 6.78 (s, 4H), 6.18 (s, 1H), 2.15 (s, 12H), 1.54 (s, 6H).

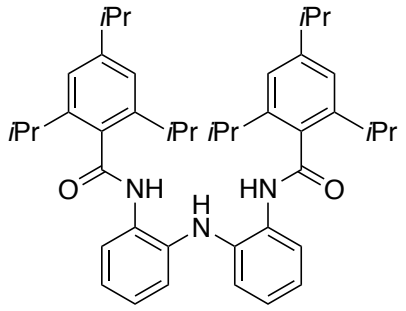

H_3L^{TRIP}

2,2'-Bis(1,3,5-triisopropylphenylacetoamido)diphenylamine [HN(*o*-PhNHC(O)(Ph(CH(CH$_3$)$_2$)$_3$)$_2$] (H_3L^{TRIP}): In a 500 mL round bottom flask, 2-nitroaniline (0.6907g, 0.005 mol) and 1-fluoro-2-nitrobenzene (0.7055g, 0.005 mol) were added and stirred in dimethyl sulfoxide (DMSO) for 15 min. Potassium tert-butoxide (1.1221g, 0.010 mol) was then slowly added to the reaction mixture. The reaction was stirred for 24 hours and then quenched by adding enough deionized water, so that all the formed bis(2-nitrophenyl)amine formed could precipitate from the solution as orange solids, which was isolated by filtration through a fritted glass filter. The orange product was washed with deionized water and *n*-hexanes and dried under vacuum. The dried orange powder was then transferred to a Parr® pressure tested hydrogenation vessel and dissolved in 30 mL of THF, and 10 wt% of Pd/C was added to the vessel. The reaction mixture was hydrogenated under H_2 (50 psi) for 30 min, followed by a quick filtration through Celite®. The filtrate was collected and concentrated under reduced pressure to yield light orange oil, to which *n*-hexanes were added. The oil and *n*-hexanes were let stirring for 3 hours and off-white solids of bis(aminophenyl)amine could be obtained, which were dried under vacuum. The dried powder was weighed and added to a 250 mL round bottom flask and let stirring in dichloromethane. To this flask, 2 equivalents of triethylamine was added, and the reaction was stirred in an ice bath for 20 min. Afterwards, 2 equivalents of 1,3,5-triisopropylbenzoyl chloride was then slowly added to the reaction mixture, which was stirred for 24 hours and allowed to

slowly return to room temperature. Extraction of the reaction mixture was then performed first with saturated aqueous sodium bicarbonate solution for three times, and then with brine solution. The organic layer was collected, dried over $MgSO_4$, filtered, and then dried to solid using a rotary evaporator. The solid was then stirred in *n*-hexanes for 3 hours, filtered, and dried under reduced pressure to obtain the final product H_3L^{TMP}, which was an off-white powder. **^{1}H NMR** (400 MHz, $CDCl_3$): δ 7.86-7.82 (m, 2H), 7.75 (s, 2H), 7.13-7.09 (m, 4H), 6.95 (s, 4H), 6.91-6.87 9m, 2H), 6.46 (s, 1H), 2.95 (p, J = 6.8 Hz, 4H), 2.84 (p, J = 6.9 Hz, 2H), 1.20 (d, J = 6.9 Hz, 12H), 1.16 (d, J = 6.8 Hz, 12H), 1.04 (d, J = 6.8 Hz, 12H).

Isolation of complexes

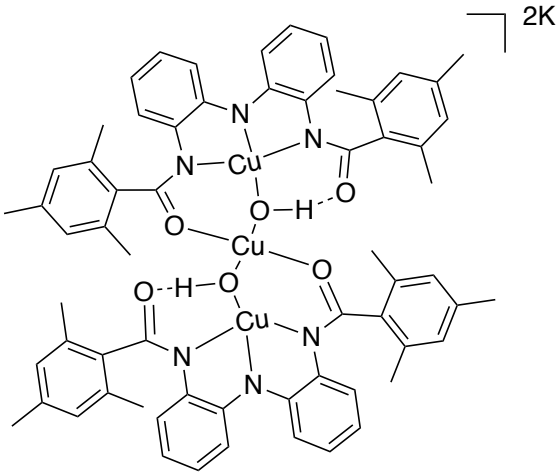

$K_2[Cu^{II}_3(L^{TMP})_2(OH)_2]$

$K_2[Cu^{II}_3(N(o\text{- }PhNHC(O)\ (Ph(CH_3)_3))_2)_2(OH)_2]$ ($K_2[Cu^{II}_3(L^{TMP})_2(OH)_2]$:

Method A: In a 20 mL vial in the glovebox, H_3L^{TMP} (24.56 mg, 0.05 mmol), and KH (6.42 mg, 0.16 mmol) were added to a solution of anhydrous dimethylformamide (DMF). The reaction was let stirring for 30 min until no bubbles of H_2 could be observed. $CuBr_2$ (11.17 mg, 0.05 mmol) was then added to the mixture. The reaction was stirred for 24 hours before DMF was removed under reduced pressure. The dried sample was redissolved in anhydrous acetonitrile to

precipitate KBr. After filtering the sample through fritted glass filter, the filtrate was collected and dried under reduced pressure. Anhydrous *n*-hexanes were added to the dried sample, and it was stirred for 3 hours. Grey-green powder formed in the solution, which was filtered, washed with *n*-hexanes, and dried under reduced pressure. The powder was dissolved in acetonitrile and put in the freezer for slow evaporation. Dark orange crystals that were almost black grew out of the solution, which was confirmed by X-ray diffraction to be $K_2[Cu^{II}_3(L^{TMP})_2(OH)_2]$ (see Table 3-4 for crystallographic data).

Method B: In a 20 mL vial in the glovebox, H_3L^{TMP} (24.56 mg, 0.05 mmol), and KH (6.42 mg, 0.16 mmol) were added to a solution of anhydrous dimethylformamide (DMF). The reaction was let stirring for 30 min until no bubbles of H_2 could be observed. $CuBr_2$ (11.17 mg, 0.05 mmol) was then added to the mixture. The reaction was stirred for 24 hours before DMF was removed under reduced pressure. The dried sample was redissolved in anhydrous acetonitrile to precipitate KBr. After filtering the sample through fritted glass filter, the filtrate was collected and dried under reduced pressure. Anhydrous *n*-hexanes were added to the dried sample, and it was stirred for 3 hours. Grey-green powder formed in the mixture was filtered, washed with *n*-hexanes, and dried. Diethyl ether was then added to the mixture, and most of the product was dissolved, forming a dark yellow solution. The solution was set aside for slow evaporation at room temperature, from which crystals of $K_2[Cu^{II}_3(L^{TMP})_2(OH)_2]$ grew.

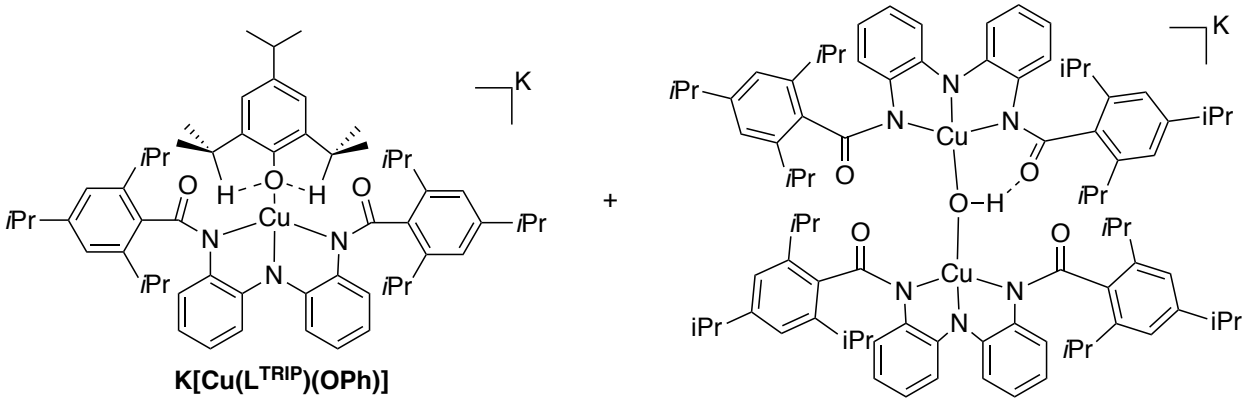

K[Cu(L^{TRIP})(OPh)] **K[Cu$_2$(OH)(L^{TRIP})$_2$]**

K[Cu(N(*o*- PhNHC(O)(Ph(CH(CH$_3$)$_2$)$_3$))$_2$)(OPh(CH(CH$_3$)$_2$)$_3$)] (K[Cu(L^{TRIP})(OPh)]) and K[Cu$_2$(N(*o*- PhNHC(O)(Ph(CH(CH$_3$)$_2$)$_3$))$_2$)$_2$(OH)] (K[Cu$_2$(OH)(L^{TRIP})$_2$]): In a 20 mL vial in the glovebox, H_3L^{TRIP} (32.97 mg, 0.05 mmol), and KH (6.42 mg, 0.16 mmol) were added to a solution of anhydrous dimethylformamide (DMF). The reaction was let stirring for 30 min until no bubbles of H_2 could be observed. $CuBr_2$ (11.17 mg, 0.05 mmol) was then added to the mixture. The reaction was stirred for 24 hours before DMF was removed under reduced pressure. The dried sample was redissolved in anhydrous acetonitrile to precipitate KBr. A portion of the mixture remained unfiltered and was set aside at room temperature for slow evaporation, from which crystals that were almost black grew. These crystals were confirmed by X-ray diffraction to be K[Cu(L^{TRIP})(OPh)] (see Appendix for crystallographic data). The other portion of the mixture was filtered, dried under reduced pressure, and stirred in *n*-hexanes for 3 hours. The dark purple powder formed in the stirred mixture was filtered, dried, and redissolved in diethyl ether. A portion of the product was insoluble in diethyl ether, which was filtered, dried, and dissolved in acetonitrile. The sample was then put in the freezer for slow evaporation, and dark crystals were obtained, which were confirmed by X-ray diffraction to be K[Cu_2(OH)(L^{TRIP})$_2$] (see Table 3-4 for crystallographic data).

Table 3-4. Crystallographic data for complexes **4**, **6**, and **7**.

	4	**6**	**7**
Empirical formula	$C_{76}H_{80}Cu_3K_2N_{12}O_6$	$C_{61}H_{80}CuKN_4O_3$	$C_{96}H_{121}Cu_2KN_{10}O_5$
Formula weight	1526.39	1019.93	1661.20
T (K)	100	106	106
λ (Å)	1.5414	1.54184	1.54184
Crystal size (mm^3)	0.29 x 0.28 x 0.23	0.21 x 0.11 x 0.07	0.42 x 0.32 x 0.18
Crystal system	Monoclinic	Triclinic	Triclinic
Space group	C2/*c*	P-1	P-1*c*
a (Å)	25.2075	13.2995	14.392
b (Å)	11.7515	14.6275	17.7146
c (Å)	27.5372	16.0196	1.1521
α (º)	90.156	98.331	82.033
β (º)	112.416	107.197	86.646
γ (º)	9.62	105.978	76.433
V ($Å^3$)	7540.7	2993.9	4592.1
Z	4	2	2
δ_{calc} (g/m^3)	1.345	1.221	1.201
GOF on F^2	1.055	1.030	1.020
*R*1, *wR*2 [$I > 2\alpha(I)$]	0.0676, 0.1829	0.0775, 0.18894	0.0458, 0.1242

References

1. Holland, P. L.; Cundari, T. R.; Perez, L. L.; Eckert, N. A.; Lachicotte, R. J. *J. Am. Chem. Soc.* **2002**, *124*, 14416-14424.

2. Baenziger, N. C.; Dittemore, K. M.; Doyle, J. R. *Inorg. Chem.* **1974**, *14*, 805-811.

3. Sharma, S. K.; May, P. S.; Jones, M. B.; Lense, S.; Hardcastle, K. I.; MacBeth, C. E. *Chem. Commun.* **2011**, *47*, 1827-1829.

4. Lo Presti, E.; Perrone, M. L.; Santagostini, L.; Casella, L.; Monzani, E. *Inorg. Chem.* **2019**, *58*, 7335-7344.